AD-A127 016 MITHRAS: A PROGRAM OF SIMULTANEOUS RADAR OBSERVATIONS OF THE HIGH-LATITUD..(U) SRI INTERNATIONAL MENLO PARK CA O DE LA BEAUJARDIERE ET AL. NOV 82 AFOSR-TR-83-0238 1/1

UNCLASSIFIED F49620-81-C-0042 F/G 4/1 NL

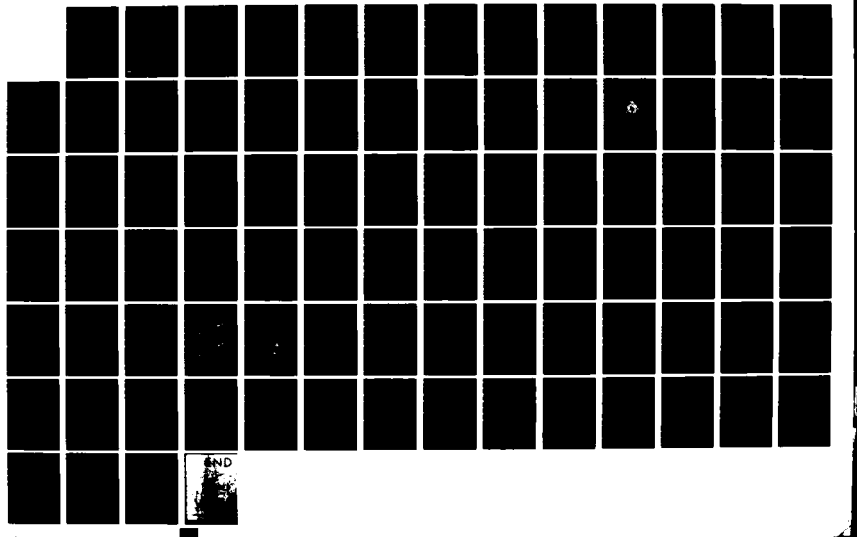

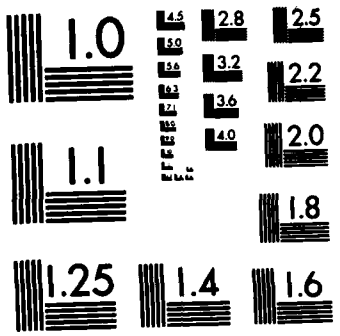

MICROCOPY RESOLUTION TEST CHART
NATIONAL BUREAU OF STANDARDS-1963-A

Final Scientific Report *November 1982*

MITHRAS:

A Program of Simultaneous Radar Observations of the High-Latitude Auroral Zone

By: O. de la BEAUJARDIERE M. J. BARON V. B. WICKWAR
C. SENIOR J. V. EVANS

Prepared for:

DEPARTMENT OF THE AIR FORCE
AIR FORCE OFFICE OF SCIENTIFIC RESEARCH (AFSC)
BOLLING AIR FORCE BASE
WASHINGTON, DC 20332
Attention: LT. COL. TED CRESS

CONTRACT F49620-81-C-0042

SRI Project 3261

333 Ravenswood Avenue
Menlo Park, California 94025 U.S.A.
(415) 326-6200
Cable: SRI INTL MPK
TWX: 910-373-2046

SRI International®

SRI International

Final Scientific Report
Covering the Period 1 May 1981 to 30 September 1982

November 1982

MITHRAS:

A Program of Simultaneous Radar Observations of the High-Latitude Auroral Zone

By: O. de la BEAUJARDIERE M. J. BARON V. B. WICKWAR
C. SENIOR J. V. EVANS

Prepared for:

DEPARTMENT OF THE AIR FORCE
AIR FORCE OFFICE OF SCIENTIFIC RESEARCH (AFSC)
BOLLING AIR FORCE BASE
WASHINGTON, DC 20332
Attention: LT. COL. TED CRESS

CONTRACT F49620-81-C-0042

SRI Project 3261

Approved by:

ROBERT S. LEONARD, *Director*
Radio Physics Laboratory

DAVID D. ELLIOTT, *Vice President*
Research and Analysis Division

333 Ravenswood Avenue • Menlo Park, California 94025 • U.S.A.
(415) 326-6200 • Cable: SRI INTL MPK • TWX: 910-373-2046

Unclassified

SECURITY CLASSIFICATION OF THIS PAGE (When Data Entered)

REPORT DOCUMENTATION PAGE

READ INSTRUCTIONS BEFORE COMPLETING FORM

1. REPORT NUMBER: AFOSR-TR- 83-0238

2. GOVT ACCESSION NO.: AD-A127 006

3. RECIPIENT'S CATALOG NUMBER:

4. TITLE (and Subtitle)

MITHRAS: A PROGRAM OF SIMULTANEOUS RADAR OBSERVATIONS OF THE HIGH-LATITUDE AURORAL ZONE

5. TYPE OF REPORT & PERIOD COVERED: Final Scientific Report

6. PERFORMING ORG. REPORT NUMBER:

7. AUTHOR(s)

O. de la Beaujardiere, M. J. Baron, V. B. Wickwar, C. Senior, and J. V. Evans

8. CONTRACT OR GRANT NUMBER(s): F49620-81-C-0042

9. PERFORMING ORGANIZATION NAME AND ADDRESS

SRI International
333 Ravenswood Avenue
Menlo Park, CA 94025

10. PROGRAM ELEMENT, PROJECT, TASK AREA & WORK UNIT NUMBERS: 61102F 2310/A2

11. CONTROLLING OFFICE NAME AND ADDRESS

Department of the Air Force
Air Force Office of Scientific Research (AFSC)/NC
Bolling AFB, Washington, D.C., 90332

12. REPORT DATE: November 1982

13. NO. OF PAGES: 86

14. MONITORING AGENCY NAME & ADDRESS (if diff. from Controlling Office)

15. SECURITY CLASS. (of this report): Unclassified

15a. DECLASSIFICATION/DOWNGRADING SCHEDULE

16. DISTRIBUTION STATEMENT (of this report)

[illegible]; d.

17. DISTRIBUTION STATEMENT (of the abstract entered in Block 20, if different from report)

18. SUPPLEMENTARY NOTES

19. KEY WORDS (Continue on reverse side if necessary and identify by block number)

Auroral zone
Incoherent-scatter radar
Substorms
Joule heating
Conductivities
Thermosphere
Electric fields
Magnetosphere
Ionosphere

20. ABSTRACT (Continue on reverse side if necessary and identify by block number)

An intensive campaign of coordinated incoherent-scatter radar experiments took place in 1981-1982. It was planned to take advantage of the short period during which three incoherent-scatter radars could probe the auroral zone simultaneously. The three incoherent-scatter radars that participated in the MITHRAS experiments were Chatanika, Millstone-Hill, and EISCAT. Collaborative studies were undertaken using data from the DE spacecraft and the STARE radar. There were three main types of MITHRAS experiments, each with a different scientific purpose. MITHRAS #1 was aimed at large latitudinal coverage of F-region drifts, electron-densities, and

DD FORM 1 JAN 73 1473
EDITION OF 1 NOV 65 IS OBSOLETE

Unclassified
SECURITY CLASSIFICATION OF THIS PAGE (When Data Entered)

19. KEY WORDS (Continued)

20 ABSTRACT (Continued)

temperatures. MITHRAS #2 was designed for very good height and time resolution. MITHRAS #3 was intermediate between the other two modes. It provided both E- and F-region coverage over several degrees in latitude.

Under the MITHRAS project, substantial changes and additions were made to the software and hardware systems at Millstone and Chatanika.

Thirty-three MITHRAS experiments were performed. Most of the data have been reduced. The analysis and interpretation of the data are well underway. Some of the scientific accomplishments are:

(1) Ionosphere--Ionospheric densities and temperature were compared for the three radars for selected periods, and between the radar and a model (RADC model). A study of Joule heating in the F region revealed the importance of the electron density in ion drag and in neutral-wind morphology.

(2) Thermosphere--A method was developed to determine the auroral zone altitude profiles of neutral parameters such as temperature and oxygen concentration. Thermospheric parameters were obtained for several periods, and the EISCAT and Chatanika values compared.

(3) Magnetosphere--Detailed case studies dealt with the effect of substorms on convection. A three-radar comparison of the substorm signature in the electric field revealed that the signature depends primarily on the local time where the observation is made. Intense electric fields associated with substorms can be a predominant factor in the formation of ionospheric troughs. Subauroral electric fields were observed during a period of prolonged magnetic activity, and interpreted in terms of ring-current shielding.

(4) Empirical Models--Models were constructed to characterize the day and night conductivities, the electric fields, the E- and F-region densities, and the exospheric temperature. These models yield averaged values of the observed radar parameters as a function of quantities such as K_p, solar flux, IMF, solar zenith angle, or precipitation.

(5) Theoretical Model--A theoretical model of the temporal variation and global effects of ring-current shielding was developed.

Scientific collaborations between the various groups took place informally and during MITHRAS working meetings. A number of data tapes were exchanged among groups. This exchange of data was facilitated by the implementation of a general data format.

Related to MITHRAS, there were 12 scientific publications, and 14 papers presented at international conferences.

CONTENTS

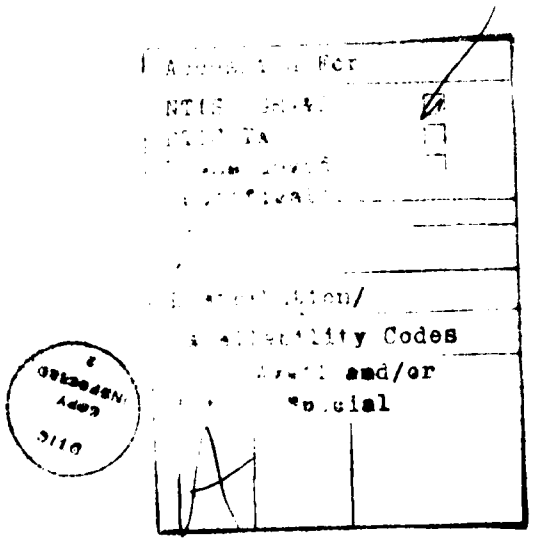

ILLUSTRATIONS

TABLES

I INTRODUCTION

For about six months, the high-latitude ionosphere could be probed simultaneously from three incoherent-scatter facilities widely separated in longitude. To take advantage of this opportunity, an intensive program of coordinated experiments began in May 1981 and ended in March 1982 when the Chatanika radar was relocated in Greenland. The three incoherent-scatter radars able to study simultaneously the auroral zone were Chatanika, Millstone Hill, and the European Incoherent-Scatter Facility (EISCAT). As illustrated in Figure I-1, the Chatanika and EISCAT radars are more than eleven hours apart, and Millstone Hill is roughly midway between them. Because the duration of the window during which the three incoherent-scatter facilities were operational was so short, the period of simultaneous observations was extended on both ends by two-radar experiments. EISCAT came on line in August 1981. Measurements from the Scandinavian Twin Auroral Radar Experiment (STARE) were utilized throughout the campaign. STARE operates continuously and can measure electric fields over a large portion of Scandinavia.

The coordinated experiments were motivated by a need to understand the coupling between the magnetosphere, the ionosphere, and the thermosphere. Because the magnetic field lines that emerge near the earth's pole connect to very distant regions of the earth's magnetosphere, the auroral zone may be thought of as a viewing screen on which much of the magnetosphere can be examined. Currents and high-energy particles propagate along these field lines, to a first approximation, and the magnetospheric electric-fields map into the ionosphere along these lines. These high-latitude regions have long been of interest as a means of diagnosing the behavior of the distant magnetosphere. The energy transfer between the magnetosphere takes place in the auroral zone via particle precipitation, Joule heating, and ion drag. Most of this energy, which totals 10^{18} to 10^{19} ergs/s, eventually goes into heating the neutral atmosphere.

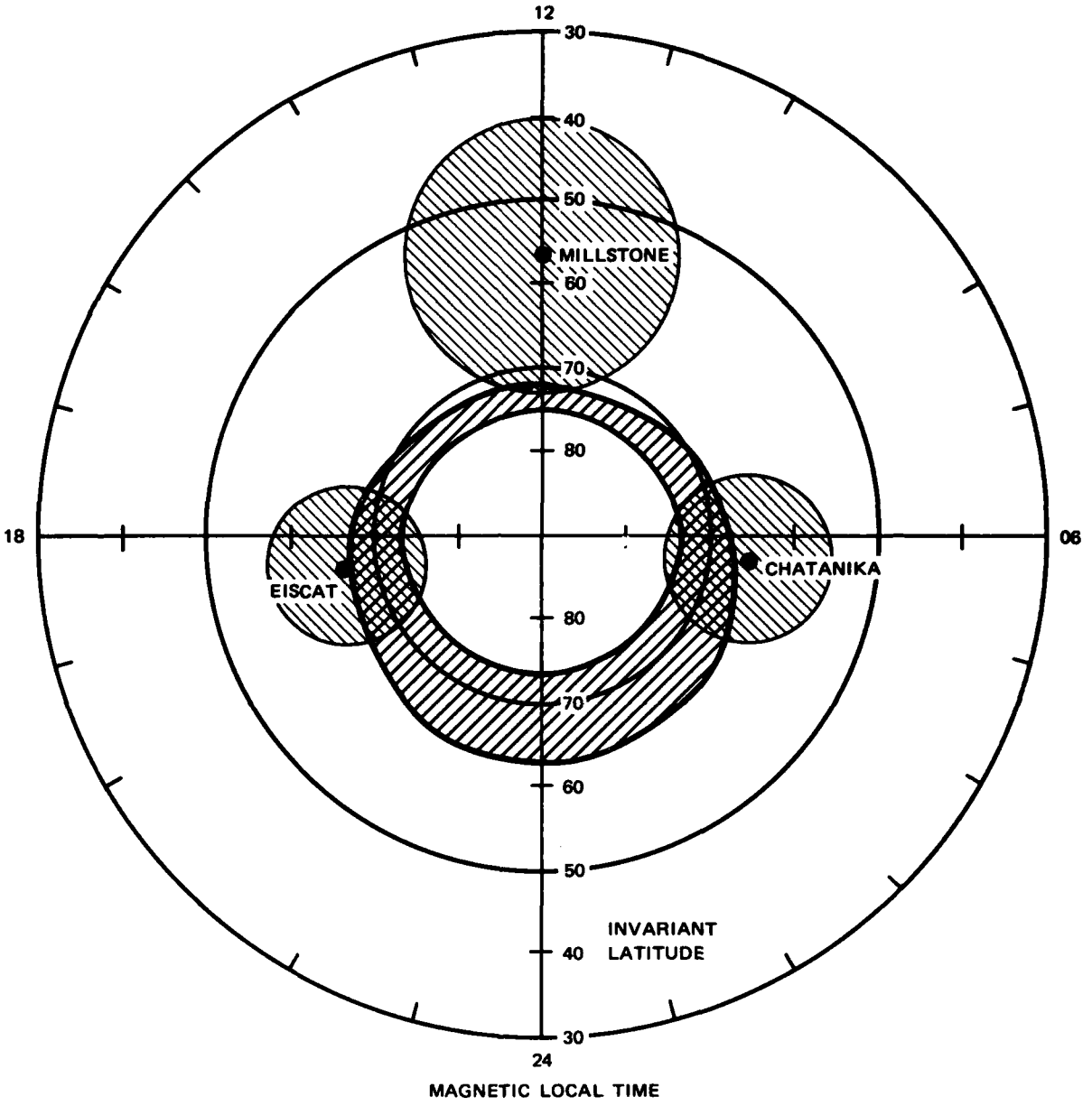

FIGURE I-1(a) MLT-INVARIANT LATITUDE PLOT OF THE POSITIONS OF THE EISCAT, CHATANIKA, AND MILLSTONE HILL RADARS WHEN MILLSTONE HILL IS AT MAGNETIC NOON. The auroral oval is that of Feldstein [1968], for moderate activity (Q = 5). The small circles represent the F-region area probed at 500-km altitude and with an elevation of 4°, 20°, and 20° for Millstone, Chatanika, and EISCAT, respectively. MLT was computed for the the month of June.

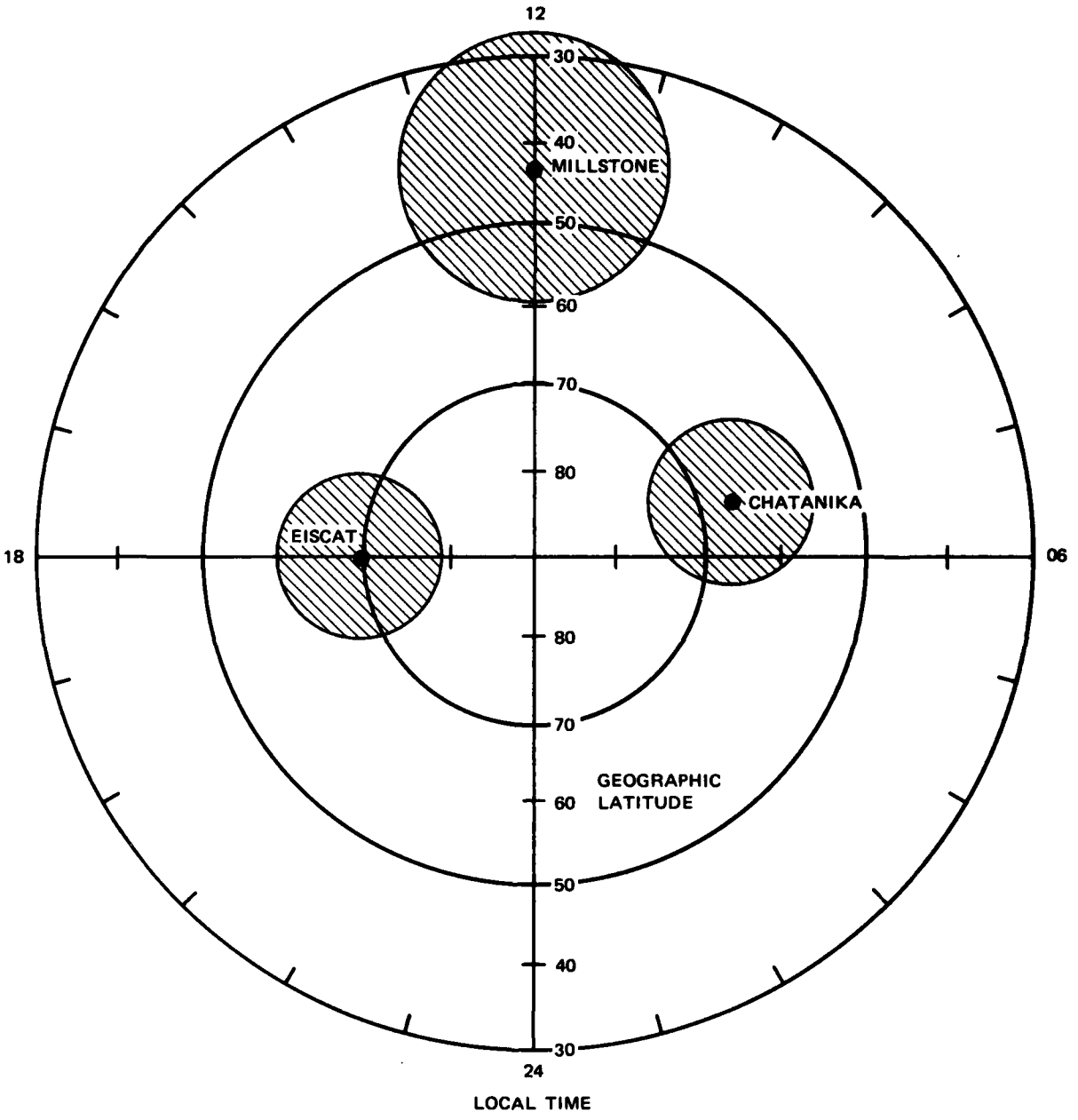

FIGURE I-1(b) LOCAL TIME VERSUS GEOGRAPHIC LATITUDE OF EISCAT, CHATANIKA, AND MILLSTONE HILL RADARS, WHEN MILLSTONE HILL IS AT LOCAL NOON

The auroral zone is not a passive element in the magnetosphere-ionosphere system; it influences the magnetospheric time-dependent behavior. The field-aligned currents, for example, close in the ionosphere through Hall and Pedersen currents. The magnitude of these currents depends on conductivities, which are a function of electron densities. Gradients in conductivity result in polarization electric fields that map back into the magnetosphere; field-aligned currents may be generated in the region of conductivity gradients to keep the total current divergence free. Neutral winds exert a dynamo action on the magnetosphere-ionosphere electrodynamic coupling. It follows that the upper atmosphere forms a dynamically coupled system of considerable complexity. This complexity has greatly hindered efforts to fully understand how the interactions take place. Separating cause and effect, for example, is often difficult. For this reason a proper combination of detailed and complete observations, together with theoretical modeling, is now considered necessary if progress is to be made.

The incoherent-scatter technique is a powerful tool for ionospheric research. The phenomena that can be studied using this technique in the auroral zone include ion convection, discrete and diffuse auroras, the midlatitude trough, field-aligned currents, and neutral circulation. The study of these large-scale processes from two or more stations, widely separated in longitude, but at the same invariant latitude, can provide important new information about the global behavior of the ionosphere, the magnetosphere, and the thermosphere. When using one instrument alone, questions arise persistently in the interpretation of the observations. These questions involve local time/universal time (LT/UT) ambiguities or, equivalently, space/time differences. it is only with simultaneous observation from several stations that some of these ambiguities can be overcome.

To acquire data relevant to these questions, the Air Force Office of Scientific Research (AFOSR) funded the MITHRAS* program at SRI

*MITHRAS (Magnetosphere Ionosphere Thermosphere Radar Studies) was the ancient Persian god of light and truth, opponent of darkness and evil (Webster's New Collegiate Dictionary).

International from 1 May 1981 to 30 September 1982. This funding enabled the Chatanika and Millstone Hill radars to almost triple the number of simultaneous operating hours. The observations were coordinated with those at EISCAT and arrangements were made to collaborate and exchange data with EISCAT scientists. In addition, a data exchange agreement between SRI International and the STARE radar was negotiated. Similarly, arrangements were made for the Dynamics Explorer (DE) satellites to operate during MITHRAS observations.

For the MITHRAS program, the specific tasks to be accomplished were the following:

- Plan and coordinate a program of joint experiments to study the auroral region of the earth's ionosphere using the Chatanika, Millstone Hill, and EISCAT incoherent-scatter radars.
- During the period when both Chatanika and EISCAT are jointly operational, conduct additional coordinated observations at Chatanika at a rate more than double the present one; and, through a subcontract to the MIT Haystack Observatory, provide for doubling the observations at Millstone Hill.
- Devise mutually agreeable formats for the reduced data and provide for the storage of the Chatanika and Millstone coordinated data in a data library at SRI International.
- Secure an exchange of data between EISCAT and the United States to produce complete data sets here and in Europe.
- Analyze the data collected at Chatanika.
- Examine the results of the joint experiments to ensure that the scientific objectives are being met and, if not, suggest improvements to the experimental procedures or the data reduction methods.
- Develop techniques and models for comparing the data sets.
- Apply these techniques and models to scientific problems.
- Cooperate with other interested scientists as appropriate.

In this report we give a brief description of the various aspects of the research. Section II describes the instrumentation and the hardware and software modifications done under the contract. The MITHRAS experimental modes and their specific purposes are then characterized. This section also includes the catalogue of all MITHRAS observations.

Section III describes the scientific results as they relate to the ionosphere, the thermosphere, and the magnetosphere. The empirical and theoretical modeling efforts in progress are also described. This section is aimed at giving an overview of the results rather than a lengthy scientific treatise. Details on the scientific results can be found in the publications related to MITHRAS listed in Appendix B.

Section IV deals with the interchange of data, the MITHRAS meetings and workshop and the various collaborations that are taking place. Section V summarizes the work performed under the contract.

II EXPERIMENTS

A. Instrumentation

1. The Radars

The Chatanika radar is described in Leadabrand et al. (1972)* and the techniques to infer ionospheric parameters from the directly observed parameters are documented in Wickwar (1975), and de la Beaujardiere et al. (1980). The upgraded Millstone Hill radar has been documented by Evans et al. (1980). The EISCAT system is described in Folkestadt et al. (1982). While Chatanika and Millstone are monostatic, EISCAT is tristatic. It is composed of a transmitter and receiver station in Tromso, Norway, and of receiving stations in Kiruna, Sweden, and Sodankyla, Finland.

Some of the parameters that can be deduced from incoherent-scatter observations are: electron density, electric field, ionospheric current, magnetic field-aligned current, energy deposition rates, ion and electron temperature. With STARE, only electric fields are available. They are obtained from the two backscatter radar doppler-shifted echoes that arise when the fields are above a threshold (Greenwald et al., 1978).

Chatanika and EISCAT are well located for auroral zone observations (Table II-1 lists the geographic and geomagnetic coordinates of the three radars). Figures I-1(a) and II-1 show that the invariant latitudes of the two facilities are almost the same. For average magnetic activity, both radars are under the auroral oval during most of the night. During the day, they are slightly south of it. Chatanika leads EISCAT by about eleven hours in magnetic local time (MLT). The small circles in Figure I-1 represent the F-region area covered by the radars.

*References are listed, alphabetically, at the end of this report.

Table II-1

COORDINATES FOR CHATANIKA, EISCAT, AND MILLSTONE HILL FACILITIES

Parameter	Chatanika	EISCAT (Tromsø)	Millstone Hill
Geographic latitude	65.1° N	69.5°N	42.6°N
Geographic longitude	147.5°W	19.2°E	71.5°W
Invariant latitude, Λ	65.1°	66.3°	57.0°
Dipole geomagnetic longitude	105°W	105°E	1.5°W
Λ coverage at 350-km altitude	56° to 74°	61° to 71°	42° to 70°
L value	5.6	6.2	3.0
Dip angle	77°	77.6°	70°
Declination	29°	3.2°	-14°

By comparing Figure I-1(a) and (b) we see that the longitudinal distances in local time (LT) are different than in MLT, and that, although their invariant latitudes are nearly equal, EISCAT and Chatanika lie at quite different geographic latitudes. The maps in Figures I-1(b) and II-1 show that EISCAT (at Tromso) is north of the arctic circle, whereas Chatanika is south of it. The solar illumination, which induces heating and ionization, depends on the geographic latitude, while the magnetospheric phenomena depend on the geomagnetic latitude. Thus, longitudinal variations are expected to exist in the data from the two radars, and have in fact been observed with the MITHRAS data as will be seen later.

Millstone Hill lies considerably to the south of either Chatanika or EISCAT. Accordingly, Millstone Hill can examine the E region (90-to-150-km altitude) only to about 62° invariant latitude. The F region can, however, be studied over a wide range of latitudes (Figure I-1(b)).

2. Equipment Modification

Hardware modifications were needed for the MITHRAS project both at Chatanika and Millstone Hill. At Chatanika, the receiving/

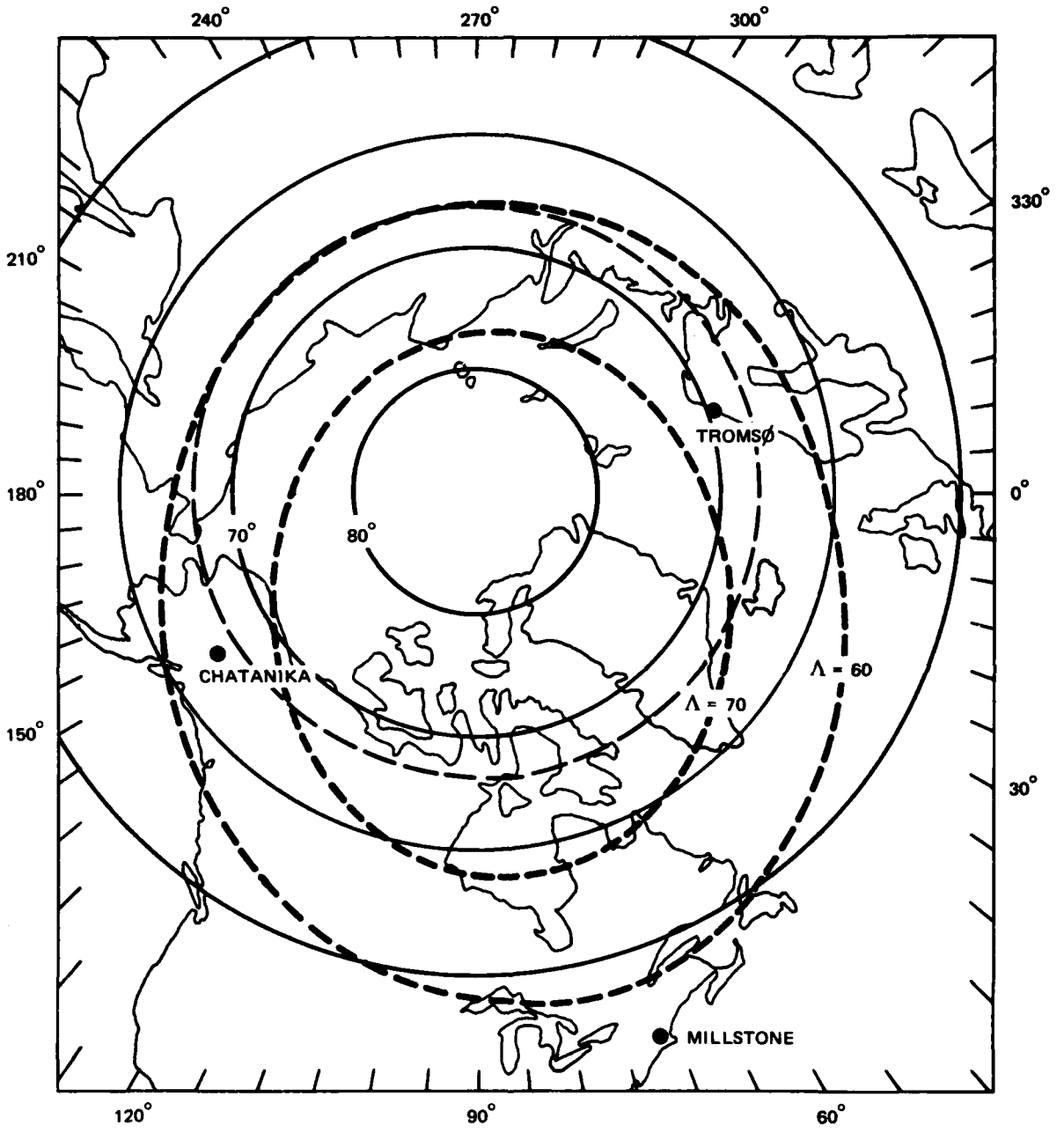

FIGURE II-1 MAP SHOWING THE LOCATION OF CHATANIKA, MILLSTONE, TROMSØ (THE EISCAT TRANSMITTER LOCATION), AND OF THE 70° AND 60° INVARIANT LATITUDE CIRCLES

processing system was modified to provide an increased bandwidth. This increase was necessary to ensure that the received signal spectrum does not partially shift out of the receiver passband because of high line-of-sight plasma velocities at low elevation angles. The modification, increasing the bandwidth from 50 kHz to 62.5 kHz, was installed in mid-June of 1981.

At Millstone Hill the Harris H-100 computer was upgraded by an additional 144 K words of MOS memory, and by a 300-Megabyte disk. The memory had to be expanded because the previous system configuration had limited real and virtual memory that placed severe constraints on the data processing. The acquisition of a disk allowed large data sets to be stored on line. This allowed for long analysis runs to be left unattended through nights and weekends, which would be impossible if data were on tape because an operator would have to be present to change tapes.

Initially, a hybrid correlator and XDS-9300 computer were used for on-line signal processing, but, in August 1981, the system was changed over to a new system employing an array processor and the Harris computer.

All these equipment modifications at Chatanika and Millstone were accompanied by substantial software changes.

B. Description of the MITHRAS Experiments

Three distinct experiments were designed and carried out for the MITHRAS program. Each experiment has a different primary objective resulting in different spatial coverages and time resolutions. To achieve the objectives of the three experiments, appropriate radar operating modes were designed for Chatanika, Millstone Hill, and EISCAT. The objectives and operating modes are outlined in Table II-2, while Tables A-1, A-2, and A-3 in Appendix A list the operating-mode details for the three radars.

Table II-2

THE THREE MITHRAS EXPERIMENTS

Experiment	Objective	Time Resolution (Min)	Chatanika Mode	Millstone Hill Mode	EISCAT Mode
#1	Widest latitudinal coverage	30 to 40	Eleven positions (5 pairs + 1 parallel to $\vec{B}$)	350° azimuth scan at 4° elevation	Several beam directions along magnetic meridian Side antennas: intersect beam in F region
#2	Shortest time resolution	10	Three positions (overhead measurements) Short-pulse correlator for E-region parameters	At two symmetric north azimuths, and for elevations 2 to 17°, E and F region measurements	Tromsø beam parallel to $\vec{B}$ side antennas; intersect at heights 110 to 700 km
#3	Intermediate time and latitude resolution	20	Elevation scan in meridian, followed by scan to the west	180° azimuth scan north of the station at 4° elevation	Same as #1

1. MITHRAS #1

This experiment was designed to provide F-region measurements with the broadest possible latitudinal coverage. The emphasis here is on large-scale studies of electric fields, temperatures and ionization. The time resolution of this experiment is 30 to 45 min.

The Chatanika radar was operated in an eleven position mode. Five pairs of positions were on either side of the magnetic meridian, and one position was parallel to $\vec{B}$, the magnetic field. Figure II-2 shows the ground projections of the eleven radar beams and of the spectral gates. With this mode a large latitudinal coverage could be achieved in the F region, and at the same time the E-region electrodynamic parameters could be determined at the radar latitude. Every hour and a half the radar was scanned in elevation in the magnetic meridian plane. This scan gave the cross-section of the ionization profile as a function of height, with a fine latitudinal resolution.

The Millstone radar was operated in an azimuth scan covering almost the full circle. The coverage achieved by the radar with this scan is illustrated on Figure II-3. This operating mode had the advantage that longitudinal effects could be studied by comparing the measurements to the east and to the west.

During the initial operations, EISCAT could only be run with simple operating modes. The mode used during this phase is described under the MITHRAS #2 experiments. In December, some latitudinal coverage was achieved with the system (M. Baron helped implement this mode during one of his visits to EISCAT). In its latest version, this mode consisted of eleven nodes along the magnetic meridian. The Sodankyla and Kiruna stations intersected the Tromso beam at 325-km altitude.

2. MITHRAS #2

This experiment was directed primarily toward substorm studies of both the E and F regions with the best possible time resolution (10 min). To realize this time resolution, which is necessary to resolve UT/LT effects, this experiment concentrated on a narrow range of latitudes near the invariant latitude of Chatanika ($\Lambda = 65°$ N). In addition

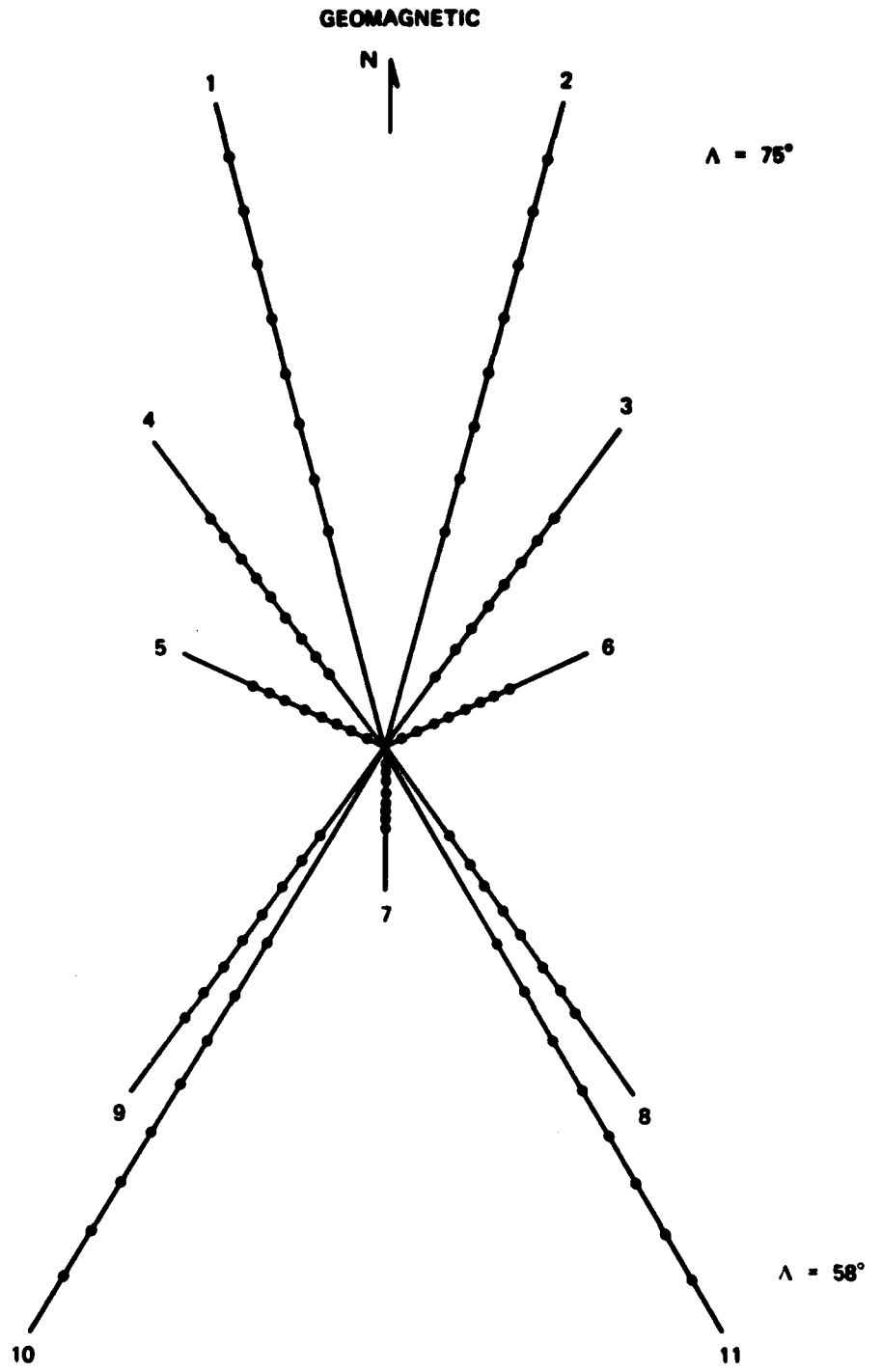

FIGURE II-2 MITHRAS # 1 EXPERIMENT AT CHATANIKA. Ground projection of the radar beams and correlator gates.

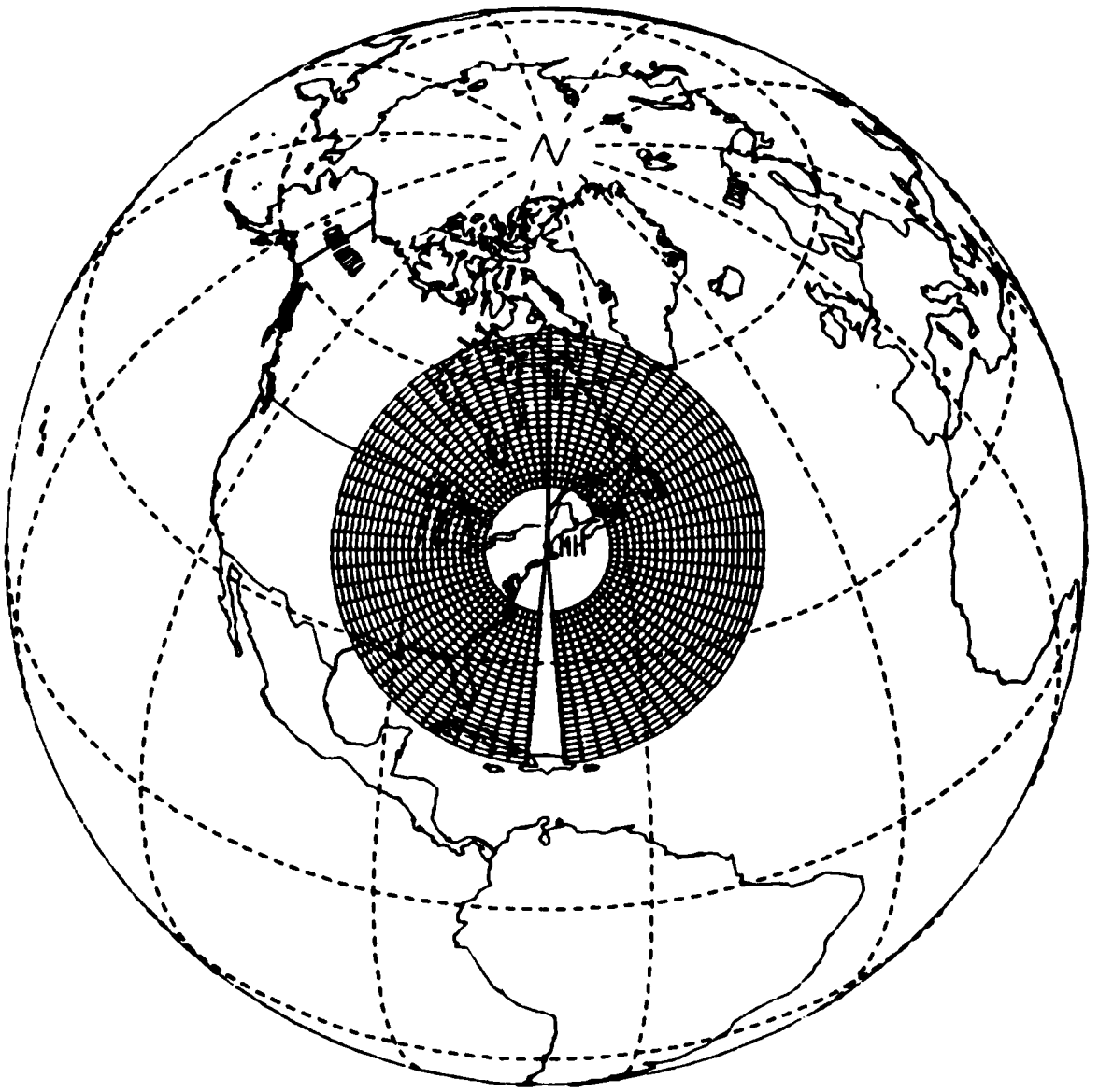

FIGURE II-3 MITHRAS # 1 EXPERIMENT AT MILLSTONE HILL. Coverage afforded by scanning the 150-ft antenna from 175° to 185° azimuth (CCW) at 4° elevation. Radial lines separate each 5° azimuth sector over which the incoherent-scatter returns are integrated, while the circles are placed at the center of each of the first 23 range gates (772-2884 km in range, corresponding to 100-800 km in altitude).

to the F-region electric fields, temperatures, and densities, E-region parameters were obtained at Chatanika and Tromso. These include conductivities, differential energy spectra of precipitating electrons, neutral winds, currents, Joule heating, and electron energy deposition rate. Note however that, even using the lowest possible elevation angle, the Millstone radar cannot probe the E region at latitudes north of $\Lambda = 62°$.

The operating mode for Chatanika consisted of a set of three positions, one parallel to the magnetic field and the two others on either side of the magnetic meridian at 70° elevation. The velocity and temperatures were obtained from two different processors, one with a fine (9-km) altitude resolution for E-region measurements, and one with a coarser (50-km) resolution for the F region.

At Millstone Hill, initial observations were conducted at 4° elevation using a 64° azimuth scan centered on the magnetic meridian. At F-region altitudes (200 to 500 km), the resulting invariant latitude coverage was 61° to 69°. The second type of MITHRAS #2 Program consisted of elevation scans from 2° to 17° at azimuths on either side of the magnetic meridian, covering the invariant latitudes from 60° to 72° for F-region altitudes. This program used a short pulse-length at the lowest elevation angles for the best possible E-region altitude resolution.

The EISCAT transmitting antenna was held fixed, parallel to the magnetic field. The two receiving stations scanned the Tromso beam at six discrete heights between 110- and 700-km altitude.

3. MITHRAS #3

This experiment was directed at examining E- and F-region morphology with a time resolution between that afforded the #1 and #2 Programs (i.e., about 20 min). For Chatanika and EISCAT it provided latitudinal coverage for both E and F regions. It was useful in identifying and following the evolution of ionization features (e.g., diffuse aurora, trough, F-region enhancements) as well as the variations of electric

field, temperatures, currents, precipitating electrons energy spectra, and the energy deposition rate associated with these features.

The Chatanika radar operated in a set of two scans. It completed one elevation scan in the magnetic meridian, then one scan to the west along a path such that, at each invariant latitude, the radar sampled the same local time that was sampled during the elevation scan. The mode for EISCAT was the same as that for MITHRAS #1. The mode used by Millstone was a 180° azimuth scan limited to the region north of the station.

C. Catalogue of MITHRAS Observations

Whenever possible, each of the three experiments described in the previous section was scheduled once a month between May 1981 and February 1982. In March 1982, after the disassembly of the Chatanika radar, one to two experiments per month continued at EISCAT and Millstone. EISCAT began coordinated MITHRAS experiments in September 1981.

A summary of MITHRAS operations at the three radars is given in Tables II-3 and II-4. The operating modes are identified by the descriptions listed in the previous section and in Appendix A. The times listed are the start and end times at each radar. There were 29 MITHRAS experiments before Chatanika was disassembled, and 4 after.

The two-way and three-way overlap hours indicate the duration of the periods when data were collected at two of the three and at all three radars. Gaps in the data caused by problems with the equipment occurred at all three stations. At Millstone Hill gaps also occurred because the radar was diverted to track satellites. Occasionally, operations had to be performed at decreased system sensitivity or with limited antenna positioning capabilities. These operations are included in the overlap time columns.

The sum of the three-hourly K_p values for each 24-hour period is listed to indicate the global magnetic conditions for the cooperative experiments. For days when two-way overlap duration exceeded 12 hours, the sum of the K_p values varied from a low of 7- to a high of 34-.

Table II-3

MITHRAS OPERATIONS

(May 1981 through February 1982)

Day Number	Date*	Time* (start-end)			Two-Way Overlap (hr)†	Three-Way Overlap (hr)†	ΣK_p	Mode
		Chatanika	Millstone Hill	EISCAT				
133	13 May	0018-2400	2135-		2.4	-	16-	MITHRAS 2
134	14 May		-0400		-	-	25	
143	23 May	1555-	1425-		8.1	-	25+	MITHRAS 1
144	24 May	-1837	-1950		13.0	-	26+	
161	10 Jun	0044-	0005-		22.7	-	9	MITHRAS 3
162	11 Jun	-0130	-0400		1.5	-	13	
174	23 Jun	2050-2340	2210-		1.5	-	10-	MITHRAS 2
175	24 Jun		-		-	-	19+	
176	25 Jun		-0400		-	-	22	
178	27 Jun	0358-	0335-		19.7	-	20-	MITHRAS 1
179	28 Jun	-0505	-1725		5.1	-	18	
185	04 Jul	0158-	0210-		20.4	-	16-	MITHRAS 1
186	05 Jul	-0358	-		4.0	-	22-	
187	06 Jul		-1215		-	-	27-	
195	14 Jul	2200-			-	-	14-	MITHRAS 2
196	15 Jul	-	1510-		8.8	-	7-	
197	16 Jul	-0012	-1520		0.2	-	16+	
202	21 Jul	2152-			-	-	13-	MITHRAS 3
203	22 Jul	-2359	0112-		17.1	-	28+	
204	23 Jul		-0030		-	-	34-	
213	01 Aug		0550-		-	-	26-	MITHRAS 1
214	02 Aug	0208-	-2330		20.8	-	22-	
215	03 Aug	-0358			-	-	26-	
218	06 Aug		0720-		-	-	21+	MITHRAS 3
219	07 Aug		0030		-	-	17+	
223	11 Aug		2005-		-	-	22+	MITHRAS 1
224	12 Aug		-		-	-	18-	
225	13 Aug		-1125		-	-	18+	
258	15 Sep		1850-		-	-	17+	MITHRAS 1
259	16 Sep		-2330	0900-	14.5	-	15-	CP‡ (-1)
260	17 Sep			-0800	-	-	9	
265	22 Sep		1318-		-	-	20	MITHRAS 3
266	23 Sep		-		-	-	8+	
267	24 Sep		-1600		-	-	16	
272	29 Sep		1949-		-	-	20+	MITHRAS 2
273	30 Sep	0130-	-	1130-	18.9	12.5	24-	CP(-1)
274	01 Oct	-0138	-0346	-0900	3.8	1.6	18	
279	06 Oct			2200-	-	-	12-	MITHRAS 3
280	07 Oct	0011-	2236-	-2120	13.4	-	32	CP(-1)
281	08 Oct	-1214	-2400		12.2	-	30	
297	24 Oct		0217-		-	-	22-	MITHRAS 1
298	25 Oct	0031	-	1630-	23.0	5.1	24+	CP(Ø)
299	26 Oct	-	-1328	-0900	13.0	8.5	18-	
300	27 Oct	-0009			-	-	18	

Table II-3 (Concluded)

MITHRAS OPERATIONS

(May 1981 through February 1982)

Day Number	Date*	Time* (start-end)			Two-Way Overlap (hr)†	Three-Way Overlap (hr)†	ΣK_p	Mode
		Chatanika	Millstone Hill	EISCAT				
300	27 Oct		2129-		-	-	18	MITHRAS 2
301	28 Oct	0004-	-		22.9	-	26	
302	29 Oct	-0200	-0415		2.0		20	
314	10 Nov	-	2130-		-	-	21-	MITHRAS 3
315	11 Nov	0000-	-	0900-1453	21.9	5.9	32-	CP(Ø)
316	12 Nov	-0213	-0135		1.6	-	30-	
321	17 Nov		2124-		-	-	33+	MITHRAS 2
322	18 Nov	0017-	-	0900-	22.6	15.0	31	CP(Ø)
323	19 Nov	-0001	-0500	-0900	5.0	-	23+	
325	21 Nov	0017-	0312-		20.5	-	23+	MITHRAS 1
326	22 Nov	-0201	-		1.9	-	19+	
327	23 Nov	-	-0926		-	-	27	
339	05 Dec	1702-	0313-		4.2	-	17+	MITHRAS 1
340	06 Dec	-1707	-0330		3.5	-	8+	
342	08 Dec	2143-	2235-	1500-	2.3	1.4	22+	MITHRAS 3
343	09 Dec	-2400	-0456	-2020	17.3	4.4	20-	CP(-3e)
349	15 Dec	2241-	2146-	1500-	2.2	1.3	10+	MITHRAS 2
350	16 Dec	-	-	-1940	21.5	17.2	9-	CP(-3s)
351	17 Dec	-0010	-0449		0.2	-	11	
9	09 Jan		0305-		-	-	8	MITHRAS 1
10	10 Jan	0620-	-		17.7	-	7-	
11	11 Jan	-0803	-1418		8.0	-	10+	
19	19 Jan	1800-	2116-		2.7	-	6+	MITHRAS 2
20	20 Jan	-2005	-	1500-2300	19.7	1.2	12+	CP(-3e)
21	21 Jan		-0458				22	
26	26 Jan	1818-	2121-	1500-	5.7	2.7	13	MITHRAS 3
27	27 Jan	-	-	-2258	24.0	21.0	21+	CP(3)
28	28 Jan	-0010	-0129		0.2	-	24	
30	30 Jan		0306-		-	-	29	MITHRAS 1
31	31 Jan	0608-	-	1000-2345	15.6	12.4	34-	CP(3)
32	01 Feb	-1320	-1332		13.3	-	34	
40	09 Feb	1550-	1042-		8.2	-	24	MITHRAS 3
41	10 Feb	-2307	-1512		15.2	-	33+	
47	16 Feb	1805-	2031-		3.5	-	13+	MITHRAS 2
48	17 Feb	-	-		23.4	-	30+	
49	18 Feb	-0003	-0459		-	-	34+	

*Dates and times are UT.

†Data gaps of > 20-min duration excluded from overlap time calculation.

‡The EISCAT Common Program (CP) modes are defined in Appendix A.

Table II-4

MITHRAS OPERATIONS: COINCIDENT MILLSTONE-EISCAT OBSERVATIONS

(March through June 1982)

Day Number	Date	Millstone Hill (UT)	EISCAT (UT)	Two-Way Overlap (hrs)	Mode	ΣK_p
114	24 Apr	0441 to 2400	- -	- -		21
115	25 Apr	0000 to 2400	1210 to 2400*	10.0	MITHRAS #1	37+
116	26 Apr	0000 to 1227	0000 to 1000	10.0	CP(3)	15-
128	8 May	0153 to 2400	- -	- -	MITHRAS #1	10
129	9 May	0000 to 2000	1018 to 2400+	8.8	CP(0)	15
130	10 May	- -	0000 to 1003	- -		11-
138	18 May	2008 to 2400	1500 to 2400	3.9	MITHRAS #3	26+
139	19 May	0000 to 2400	0000 to 2300	23.0	CP(-2)	21
140	20 May	0000 to 0358	- -	- -		17
166	15 June	2012 to 2400	- -	- -		30
167	16 June	0000 to 2400	1100 to 2400	13.0	MITHRAS #1	19+
168	17 June	0000 to 0358	0000 to 1100	4.0	CP(3)	13-

*Two hour interruption at Tromso (1614 to 1810), and problems at Tromso

+Kiruna started at 1320, and Millstone was interrupted from 1346 to 1441

When the three-way overlap lasted more than 12 hours, the ΣK_p varied from a low of 9- to a high of 34-. Fortunately, each experiment type occurred during both quiet and active geomagnetic conditions. The status of the data processing at SRI, is shown in Table II-5.

D. Software Development

1. SRI Software

Software modifications and additions were done at all levels of the data processing, virtually every program in the Chatanika processing library was modified. This work was required because the hardware was modified, or data were taken in new operating modes, or simply because the existing programs and algorithms had to be improved. Table II-6 lists under five data processing categories the various analysis programs. The Chatanika software system is described in de la Beaujardiere et al. (1980). A number of additions and changes were necessary for the MITHRAS experiments. The major programming efforts are summarized below.

EPEC--This new program was developed to compute various electrodynamic parameters from the line-of-sight velocities and electron densities. The program is very general because it derives parameters from four types of experimental modes--single position, three position, eleven position, and azimuth scan. A detailed calculation of the statistical error associated with each parameter is included in EPEC.

CHAMP--This program calculates electrodynamic parameters from MITHRAS #3 experiments. At a selected F-region altitude, it combines the two line-of-sight velocities that were sampled at the same invariant latitude, to deduce a vector electric field.

BLEDEN--This program is used to compute the electron densities and electrodynamic quantities from the data obtained during the meridian elevation scans in the MITHRAS #3 experiments. It rearranges the densities and horizontal velocities so that they are along $\vec{B}$. BLEDEN can be used as an input to CHAMP to derive electric fields, but, by itself, it can also deduce the electric field using the velocity measured in

Table II-5

CHATANIKA DATA-PROCESSING STATUS
(as of 1 October 1982)

Date	Experiment Type	PRISIS (integration, raw densities, line-of-sight velocities)	IMPEC/EPEC (E-fields, currents conductivities)	ACFIT (densities, temperatures)
13 to 14 May 81	2	yes	yes	yes
23 to 24 May 81	1	yes	yes	no
10 to 11 Jun 81	3	yes	yes	no
27 to 28 Jun 81	1	yes	yes	yes
4 to 6 Jul 81	1	yes	yes	yes
14 to 16 Jul 81	2	yes	yes	yes
21 to 22 Jul 81	3	yes	yes	no
1 to 3 Aug 81	1	yes	yes	yes
30 Sep to 1 Oct 81	2	yes	yes	yes
7 to 8 Oct 81	3	no	no	no
25 to 27 Oct 81	1	yes	yes	yes
28 to 29 Oct 81	2	yes	yes	yes
11 to 12 Nov 81	3	yes	yes	yes
18 to 19 Nov 81	2	yes	yes	yes
21 to 22 Nov 81	1	yes	yes	no
5 to 6 Dec 81	1	yes	yes	no
8 to 9 Dec 81	3	yes	yes	no
15 to 17 Dec 81	2	yes	yes	yes
10 to 11 Jan 82	1	yes	no	no
19 to 20 Jan 82	2	yes	yes	yes
26 to 28 Jan 82	3	yes	no	no
31 Jan to 1 Feb 82	1	yes	yes	no
9 to 10 Feb 82	3	yes	no	no
16 to 18 Feb 82	2	yes	no	yes

Table II-6

MAIN PROGRAMS OF THE CHATANIKA SOFTWARE SYSTEM

Program	Function
Data Collection	
HATOL	On-line data acquisition, antenna control, real-time display
First Stage: Processing and Integration	
PRISIS	Integrates data, removes instrumental effects on density channel and correlator data, derives densities and line-of-sight velocities
Second Stage: Derivation of Ionospheric Parameters	
EPEC	Calculates electric fields, conductivities, currents, neutral winds, and Joule heating from multiposition measurements
ACFIT	Calculates the ion and electron temperatures, collision frequencies, and corrected MAC and OAC* densities
PHYNALS	Calculates the fully corrected density profile from the density channel data
BLEDEN	Rearranges electron and velocity density to be along $\vec{B}$. Computes conductivities, precipitated energy, electric fields, and currents.
UNTANGLE	Calculates energy spectra of primary auroral electrons
MERWIND	Calculates F-region meridional neutral winds
CHAMP	Calculates electrodynamic parameters from MITHRAS #3 experiments
OPEC	Calculates projected horizontal velocities, conductivities, and other electrodynamic parameters corresponding to one line-of-sight. Used mainly as input for CHAMP for processing of MITHRAS #3 experiments.
TOSS4	Computes neutral atmospheric parameters: temperature, oxygen concentration. The ion Joule heating is handled correctly in some cases.

*MAC denotes short-pulse autocorrelator (4.5- to 9-km resolution)
OAC denotes long-pulse autocorrelator (48- to 60-km resolution)

Table II-6 (Concluded)

Program	Function
Plotted Displays	
TIMPLOT	Plots any series of parameters versus time
LATPLOT	Plots any series of parameters versus latitude
PROVEC	Plots profiles or vectors as a function of altitude and time
PROFILE	Plots profiles, one record per figure
RECPLOT	Displays with grey shading most parameters versus latitude and time; rectangular plot
CONBLEDN/CONTIM	Draws contours of electron density as a function of altitude and latitude, or of altitude and time
CLOCKPLT	Plots in velocity vectors; invariant latitude versus time; circular plot
GRAPLOT	Grey plots of various quantities in invariant latitude versus time; circular plot
Export Programs	Program to write specific parameters in the MITHRAS format
BLEPORT	Writes BLEDEN data in MITHRAS format. Also calculates several geometry parameters such as MLT, Λ, solar zenith angle for E and F region altitudes

both the E and F regions, following a procedure outlined by de la Beaujardiere et al. (1977). This method gives better results when the electric field is changing rapidly with time, whereas CHAMP is best used during stable conditions.

Plotting programs--Clock-dial plots of vectors, and grey-shading displays of scalar quantities were implemented. In addition, numerous improvements were added to the other plotting programs. Work has started on the library of color plotting programs to be used with the newly acquired color graphics system described below.

TOSS4--This program computes, as a function of height, the neutral temperature and the neutral oxygen concentration. It was adapted from a program developed by the group of P. Bauer and is described in Alcayde et al. (1982a,b). In this program, which is still under development, an attempt is made to take into account the Joule heating, as will be described below in Section III-B.

Calculation of Magnetic Local Time (MLT)--There are several ways to define MLT, which creates difficulties when comparing data from different instruments. We surveyed the literature, and adopted as a definition for MLT that suggested by Montbriant (1970). As we were devising the computer code to compute MLT, we noticed significant errors in Montbriant's (1970) paper. We also evaluated the difference in the value of MLT when various magnetic reference fields are utilized. This work is described in part in Baron and Hessing (1982). The resulting computer code was sent to the other MITHRAS participants.

2. Millstone Hill Software

The first nine MITHRAS experiments (up to 2 August 1981) have been processed to yield electron density, temperature, and velocities. After that, data were collected with the new Harris computer and a new radar interface. At that time, the raw data changed substantially. Instead of autocorrelation functions (ACF's), spectra were recorded. Furthermore, the separate results obtained on each of the two transmitter frequencies for each of two local oscillator mixing frequencies are

recorded. Previously, these results had been merged before recording. In addition, the number of radar range gates was increased. These changes have made it necessary to rewrite the existing data analysis program (INSCAL).

The modification of the INSCAL program was done in six steps. The first step was to develop a method for eliminating the instrumental effects in the measured spectra, and Fourier transform the spectra. This conversion is accompanied by an estimate of the error in the ACF values. The second step was to investigate the instrumental effects upon the measured spectrum. An algorithm to modify a theoretical spectrum to include these effects has been developed. The third step was to increase data storage in INSCAL to allow the increased number of spectra in each integration period. In the fourth step, the INSCAL code was modified to permit data collected with either data collection system to be included. Then the instrumental correction algorithm was implemented. Finally, the Incoherent-Scatter Data Base (ISDB) system was modified to permit storage of the increased number of ionosphere parameters determined in each integration period.

F. Acquisition of a Color Graphics Terminal

Funds were granted to upgrade the SRI computer installation by acquiring a color graphics system. Such a system is of great use to the MITHRAS program because it can generate pseudocolor data plots, produce color slides and transparencies, and print extensive computer outputs on film rather than on paper. Since the MITHRAS data from the other radars will reside at SRI, this color display will benefit the whole MITHRAS community. We will be able to use a standard format and color scale for presenting data from all the stations. This standard format should then allow greater ease, require less time, and be less costly in the comparison and analysis of data from the three facilities.

The Advanced Electronic Design, Inc. (AED) 767 intelligent color-terminal was selected as being outstanding in its field. With SRI internal funds it was coupled to a Dunn Instruments Model 631 color camera system, and a Canorama Model 380 microfiche reader printer.

The memory of the AED is 1024 × 1024 × 8 bits. An area of 768 horizontal and 575 vertical pixels can be displayed at any time. It has an "anti-aliasing" feature, which means that diagonal lines do not look like staircases. One hundred twenty colors can be used simultaneously from a palette of 2^{24} possible colors (almost 17 million!). The display window can be moved to any part of the 1024 × 1024 space. The unit includes a keyboard, a joystick, and 1:1 to 16:1 zoom. The AED 767 is a newly released unit and therefore, has benefited from technological advances. For the same approximate price, it is considerably better (in terms of number of characters, resolution, and palette) than most other currently available units.

The software integration of the color CRT to the Prime computer has progressed to the point where geophysical parameters such as electron density can be displayed as a function of time and invariant latitude.

III NEW SCIENTIFIC RESULTS

In addition to data acquisition, data reduction, and upgrades to hardware and software, considerable scientific analysis was carried out. Some of it involved quick looks at the MITHRAS data, while some of it involved an examination of earlier data to establish a context for interpretation of the MITHRAS data. This section provides an overview of what was accomplished. In some cases more detail can be found in preprints and reprints, in others the study is still preliminary and more extensive interpretation is required before submission of an article. Additional topics will also be undertaken under the new contract.

A. Ionosphere

In the auroral zone, the electron density and temperature are governed by magnetospheric effects (convection particle precipitation) thermospheric effects (neutral wind, temperature, and composition) in addition to solar extreme ultraviolet radiation (EUV). It is not always easy to determine which of these effects predominate. Because the three incoherent-scatter stations participating in MITHRAS are at different geographic latitudes, although they cover a common range of geomagnetic latitudes, the relative influence of solar, thermospheric and magnetospheric control will differ.

The MITHRAS objectives are to improve our understanding of magnetosphere/ionosphere/thermosphere coupling, and to contribute to the development of realistic models of the high-latitude ionosphere and thermosphere. Such models can be of two types: empirical (based on statistical averaging of many measurements) or theoretical (based on fundamental principles of physics). In either case, if they are to be useful, they should predict ionospheric behavior reasonably well for any given set of conditions, e.g., location, altitude, solar flux, and

magnetic activity. Models of both types have previously been developed, and are a reasonable framework in which to view the MITHRAS data.

1. Comparison with RADC-POLAR Empirical Model

One existing model is the RADC-POLAR model (Elkins, 1973). This empirical model of electron density is based on many years of data from bottom-side ionosondes and topside sounders. It has evolved and been improved since 1973, most recently by incorporating high latitude results based on Chatanika data (Vondrak et al., 1978). The RADC-POLAR model depends on sunspot number and K_p as well as solar zenith angle. For comparison we chose 27 and 28 June 1981--very near the summer solstice. Twenty-five hours of simultaneous data were obtained at Chatanika and Millstone Hill in operating modes that emphasized broad latitudinal coverage (MITHRAS #1). For the comparison described here, two invariant latitudes were chosen: $\Lambda = 61°N$ at an altitude of approximately 250 km (lower F region) and $\Lambda = 67.5°N$ at an altitude of approximately 350 km (upper F region). The geographic latitudes are significantly higher at Chatanika for the same invariant latitude. For example, at $\Lambda = 61°$, this difference is 12.4°.

The electron densities as a function of time for these two latitude/altitude pairs were compared with each other and with the predictions of the RADC-POLAR model. Figure III-1 shows the results of the comparison for the 61°N invariant latitude. The difference in diurnal variation resulting from solar control is obvious. The day-to-night density ratio is 10 to 1 at Millstone Hill, much bigger than at Chatanika where it is 5 to 1. The difference in geographic latitudes can partly explain these variations. The rapid density decay seen at Chatanika at 0800 UT is coincident with a substorm evident on the Alaska chain magnetogram. It is not clear whether the substorm is causing this decay, or whether the Chatanika field line is moving under the mid-latitude trough.

The dashed lines in Figure III-1 are the RADC-POLAR model results. For both stations, the model accurately predicts the daytime

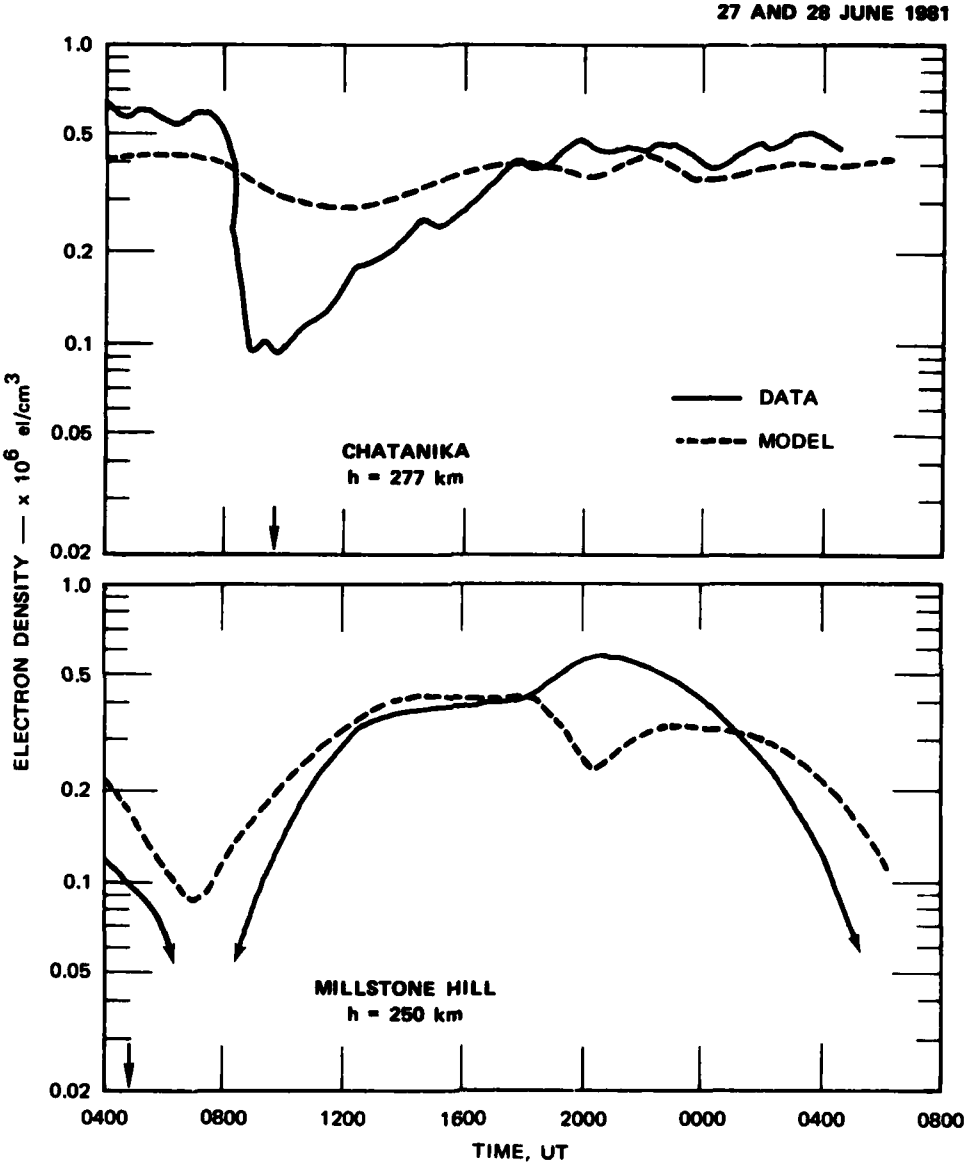

FIGURE III-1 DATA/MODEL COMPARISON FOR 61° INVARIANT LATITUDE, BELOW THE F-REGION PEAK, FOR CHATANIKA AND MILLSTONE HILL. The vertical arrow indicates local midnight.

electron densities. The nighttime minima are not as well reproduced by the model; the fit is particularly poor at Chatanika. Also, the late afternoon (2100 UT) maximum seen at Millstone Hill is not reproduced by the model.

In summary, this preliminary comparison for two invariant latitudes of electron density results from Chatanika and Millstone Hill showed that:

(1) The differing solar control of the F layer is caused by the different geographic/magnetic latitude relationship at the two sites.

(2) Perturbations due to magnetic activity are seen at both sites. For this data set, the perturbations did not occur at the same time.

When the data are compared to the RADC-POLAR model, we note that:

(1) The general agreement between the model and the day-time data is fair to good.

(2) The model does not predict a sufficiently deep nighttime minimum in the lower F region.

2. Chatanika/EISCAT Comparison of Density and Temperatures

The Chatanika and EISCAT stations are at very nearly the same invariant latitude, and EISCAT is only 4.5° higher in geographic latitude. This latter difference is less than for the above Chatanika/Millstone Hill comparison and its effect can be further minimized by choosing data from near equinox. We have chosen 30 September 1981 for a comparison of F-region ionospheric parameters. On this day the magnetic activity was comparable at the two sites (four periods of enhanced magnetic activity were observed). Thus, to the extent possible, latitudinal and magnetic-activity differences between the two locations have been minimized. Nonetheless, the electron densities behaved very differently. Figure III-2 depicts electron density contours versus altitude and time for Chatanika and EISCAT. Dissimilarities in the electron density are readily apparent. During the day, the peak electron density was larger at Chatanika than at EISCAT by almost a factor of two. During the night, on the other hand, the densities at Chatanika were smaller than at EISCAT.

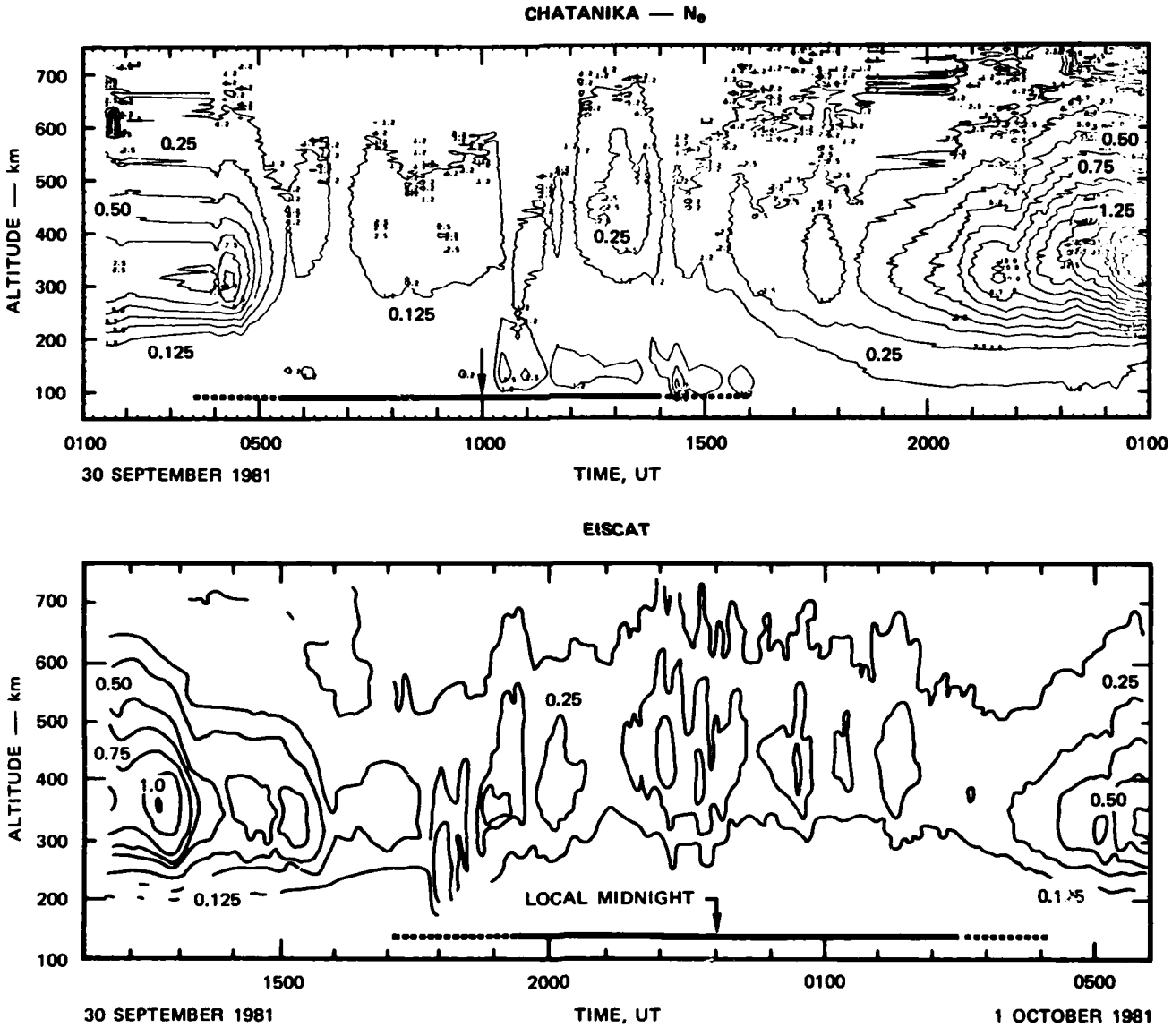

FIGURE III-2 CHATANIKA/EISCAT COMPARISON OF ELECTRON DENSITY. The vertical arrows indicate local midnight. The solid and dashed lines indicate the times during which the ionosphere above 200 km is in total darkness and at which the sun is below 90°, respectively.

A difference is also observed in the behavior at sunset and sunrise. At Chatanika, the sunset was abrupt and the sunrise very gradual. This asymmetry was not as pronounced in the EISCAT data. The Chatanika electric field increased rapidly during sunset, reaching 60 mV/m at 0515 UT. The fast decay of the F-region density may be caused by the large ion velocities and/or by the elevated ion temperatures that were also measured (Schunk et al., 1976). During sunrise, the local magnetic activity and electric fields were again enhanced at Chatanika, and the slow electron-density increase may also have been associated with the large convection.

The electron and ion temperatures were also different at both locations. These major differences in ionospheric parameters are not yet understood, but it is possible that the substorm increases in electric field and precipitation, which occurred at different local times, contributed to the differing behaviors.

3. Effect of Ion Drag on Ion Temperature

At ionospheric altitudes, interactions between the convecting ions and the neutral atmosphere result in energy transfer (Joule heating), and momentum transfer (ion drag). The energy transfer produces ion and neutral temperature enhancements; the momentum transfer can significantly modify the neutral thermospheric winds. The two effects are coupled because changes in the neutral wind velocity from ion drag will also change the amount of frictional heating of both ions and neutrals, and because Joule heating will set the air in motion due to pressure changes.

F-region ion temperature results obtained near summer solstice by the Chatanika and Millstone Hill radars were described in Baron and Wand (1982). The experimental mode was MITHRAS #1, i.e., a wide latitudinal-coverage experiment. Ion temperatures as a function of time at a fixed invariant latitude of 67.5°N were computed from two experiments, one beginning on 27 June 1981, the other on 1 August 1981. These results are summarized in the scatter plots of Figure III-3 which shows ion temperature as a function of zonal ion velocity (eastward velocities

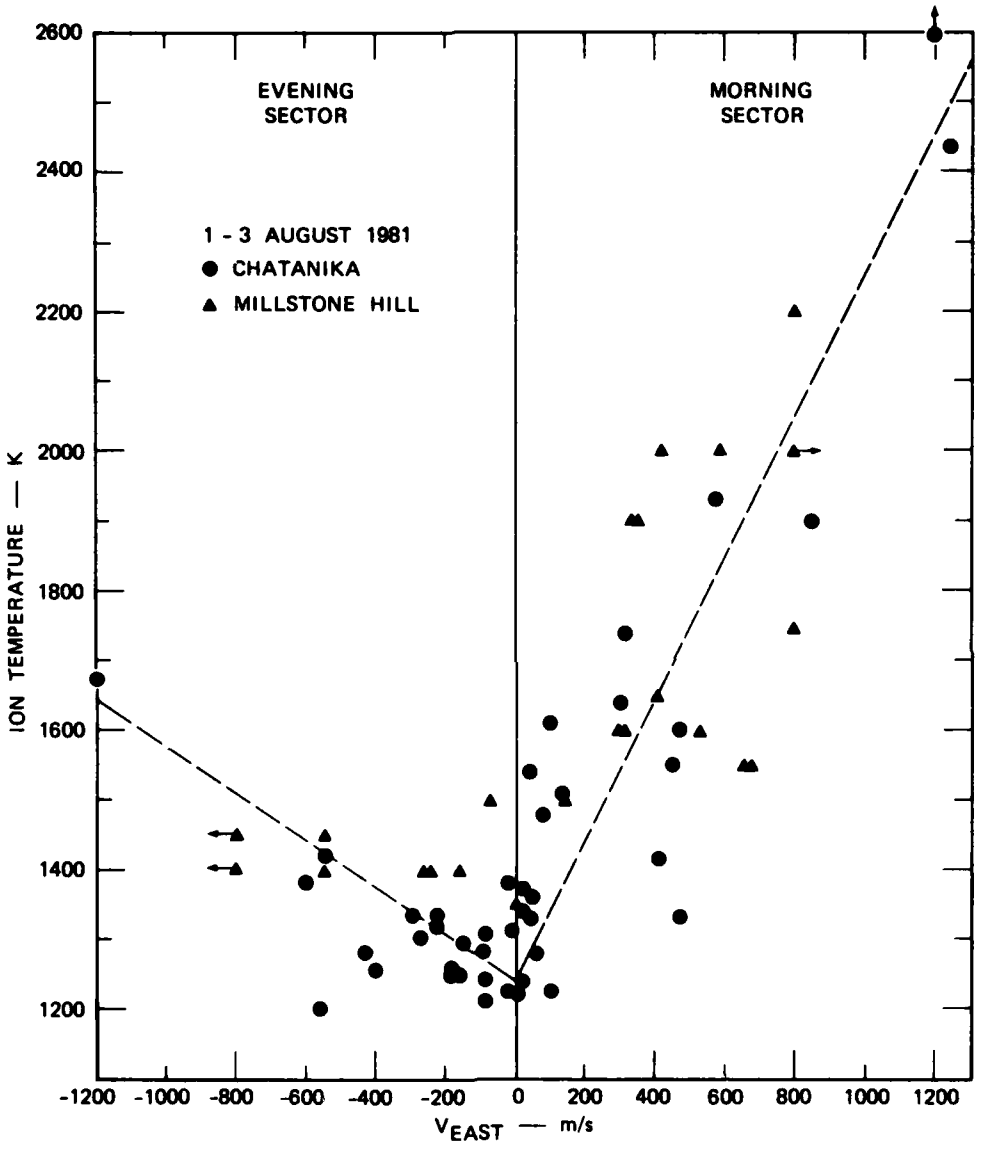

FIGURE III-3 SCATTER PLOT OF ION TEMPERATURE AS A FUNCTION OF ZONAL ION VELOCITY FOR 1 TO 3 AUGUST 1981

are positive). The circles are from the Chatanika data and the triangles from the Millstone Hill data. We clearly see that the ion temperature increases are greater for eastward than for westward velocities, i.e. greater in the morning sector than in the evening sector.

The ion temperature depends on the square of the vector-difference between the ion and neutral velocities, and hence the neutral velocity must be considered in order to understand the asymmetry of the observed morning/evening temperature enhancement.

At high latitudes, ion drag plays an important role in influencing the neutral winds. If we neglect the pressure-gradient term, and assume that above 300 km the neutral wind is constant, the momentum equation for the neutral gas is

$$\frac{\partial \bar{u}}{\partial t} = \frac{\rho_i}{\rho_n} \nu_{in} \ (\bar{v}-\bar{u}) \qquad \text{(III-1)}$$

where

ρ_i and ρ_n = ion and neutral gas densities, respectively

ν_{in} = ion-neutral collision frequency

$\bar{v}$ = ion velocity

$\bar{u}$ = neutral velocity.

Eq. (III-1) shows that the neutral velocity approaches the ion velocity exponentially with a time constant, τ, of

$$\tau = \frac{\rho_n}{\rho_i \nu_{in}} \ . \qquad \text{(III-2)}$$

To a first approximation this time constant is independent of height and inversely proportional to N_i, the ion density:

$$\tau \simeq \frac{0.226 \times 10^{10}}{N_i} \ . \qquad \text{(III-3)}$$

From Eq. III-3, τ is about 38 min for a concentration of 10^6 ions/cm^3, and 6.25 hr for a concentration of 10^5 ions/cm^3. It follows that the duration and magnitude of any ion temperature increase will depend on the ion concentration through its influence on ion drag and thus on the neutral velocity, as well as on the temporal variations of ion velocity. If the ion concentration is large, as it is likely to be in the premidnight hours when the solar-illuminated F-region has not yet decayed, then ion drag will be large, and the neutrals will be set into motion with nearly the speed of the ions within a few tens of minutes after an increase in ion drift velocity. If the ion concentration is small, as it is likely to be in the postmidnight hours, then ion drag will be small and it will take several hours for the neutrals to respond to changes in ion drift velocity. Thus, this mechanism predicts higher F-region ion temperatures in the morning sector, as observed.

In summary, simultaneous Chatanika and Millstone Hill incoherent-scatter radar measurements for two summer 24-hr periods showed that in the F region the ion temperatures were considerably larger in the morning sector than in the evening sector for similar magnitudes of ion velocity. Baron and Wand (1982) suggested that this temperature assymmetry may be in part due to ion drag, which is more effective at setting the neutrals into motion for the higher evening electron densities than for the lower morning densities. Therefore, in the evening an ion would suffer fewer random collisions, i.e. less Joule heating, and remain at a lower temperature than in the morning.

B. Thermosphere

At midlatitudes the neutral temperature and atomic oxygen concentration can be inferred from the ion energy balance in the F region (Bauer et al., 1970; Alcayde and Bauer, 1977). At high latitudes, however, this method is not valid when Joule heating occurs. An effort is now underway to overcome this limitation. This work is being done in collaboration with P. Bauer and D. Alcayde from EISCAT. The method and preliminary results are described in Alcayde et al. (1982a,b).

The SRI computer program was adapted from the code developed by the French EISCAT group. This program uses a nonlinear least-squares fitting procedure to obtain altitude profiles of the neutral temperature and oxygen concentration from profiles of electron density and electron and ion temperatures. At this time it can successfully derive the two profiles at night in the presence of Joule heating or in the presence of appreciable soft particle precipitation. However, the method is not valid when Joule heating and particle precipitation occur together.

Preliminary results were obtained for two MITHRAS days. They indicate that the exospheric temperature was nearly the same at Chatanika and EISCAT, and varied with magnetic activity. For example, on 18 November 1981, a day of high magnetic activity ($\Sigma K_p = 31$), the exospheric temperature varied between 1350 and 1450 K during the premidnight hours. These values are systematically higher than those predicted by the MSIS model (Hedin et al., 1979). This is not unexpected because the MSIS model was derived using very few high latitude data points. The application of this modified technique to the auroral region is still very new and the results must be regarded as preliminary. As confidence is gained in the technique, it will provide much new information about the high latitude neutral atmosphere and especially the response of the atmosphere to auroral inputs.

C. Magnetosphere

1. Observations on 27 June 1981: Discrete Substorms During Moderately Active Conditions

The MITHRAS data base offers a unique opportunity to observe simultaneously the auroral-zone ion convection or electric field pattern with three radars, widely separated in longitude. Our first attempt to examine local-time and universal-time effects in the electric-field signature associated with substorms is described in de la Beaujardiere et al. (1982). The period selected for this study corresponds to a day of moderate activity during which five well-defined substorms occurred. The radars at Millstone and Chatanika were operated in the MITHRAS #1 mode. EISCAT was not yet on line, but STARE was operating. The

ground-based magnetograms showed that during the observation period--0400 UT, 27 June to 0400 UT, 28 June 1981--five separate substorms occurred.

As an example of the ion convection measured on this day, Figure III-4 displays the Chatanika ion velocity vectors as a function of UT and invariant latitude. The times of each of the five substorms are indicated. Substorm #1 occurred very soon after the beginning of the experiment while Chatanika was in the dusk sector. It corresponded to both an intensification of the westward convection and a southward motion of the auroral zone equatorward boundary. Substorm #2 occurred in the midnight sector and was correlated with a temporary reversal of the convection at invariant latitudes north of 65°. Substorm #3 occurred while the radar was in the dawn sector. Its signature was an abrupt intensification of the eastward convection (1615 UT). Also, the boundary of the polar-cap convection moved to higher latitudes, i.e. poleward of the region probed by the radar. Substorm #4 occurred while the radar was in the noon sector. Although the ion velocity was small at the latitude probed by the radar, this substorm seemed to correspond to a reversal of the east-west flow.

The STARE and Millstone Hill data showed the same effects in the convection pattern as Chatanika when they were in the same local-time sectors. In addition, during Substorm #3 STARE was in the evening sector while Chatanika was in the dawn sector. Within the time resolution of the measurements, they observed a simultaneous increase in the sunward convection.

Using satellite data, Reiff et al. (1981) showed that Φ, the electrostatic potential variation across the polar cap, is proportional to the IMF parameter $\varepsilon = vB^2\sin^4(\theta/2)$ (Perreault and Akasofu, 1978), where v is the solar wind velocity, B is the magnitude of the magnetic field, and θ is the angle it makes with the earth's magnetic dipole. ε is a measure of the rate at which energy is transferred from the solar wind to the magnetosphere.

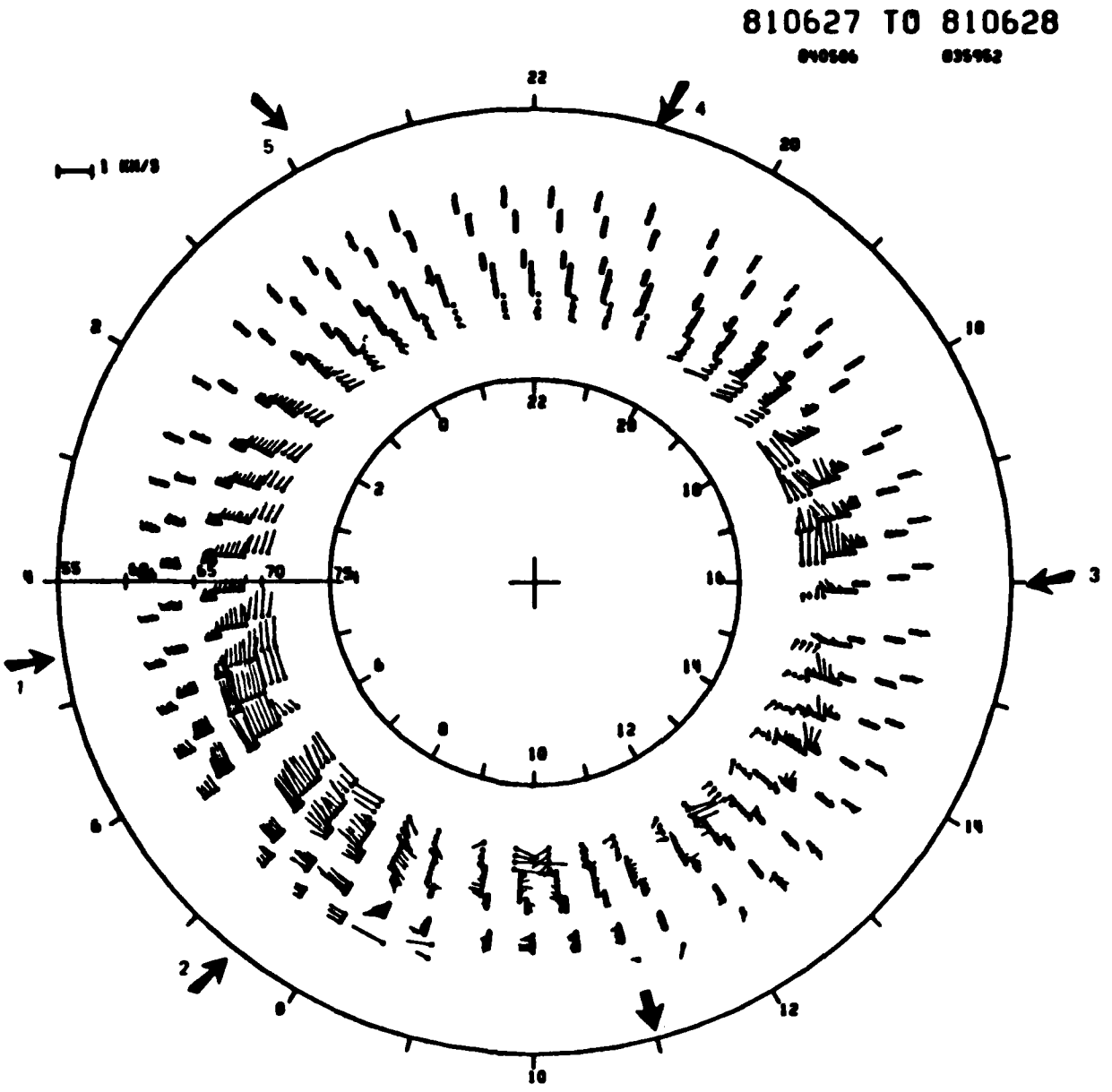

(a) CHATANIKA CONVECTION FOR
27 AND 28 JUNE 1981

FIGURE III-4 ION CONVECTION AS A FUNCTION OF INVARIANT LATITUDE AND TIME FOR CHATANIKA. The heavy arrow indicates magnetic midnight. The time is in UT. The substorms are numbered 1 through 5.

We tried to estimate Φ from the incoherent-scatter data. We assumed that in the dusk and dawn sectors, most of the auroral-zone sunward flow is within the field of view, and that the convection pattern is formed by two symmetric cells. With these assumptions, the potential across the auroral zone is half of the cross polar-cap potential. Using solar-wind data from the ISEE-1 and -3 spacecrafts (C. Russell, private communication) we compared our values of Φ versus ε with those of Reiff et al. (1981). The three crosses on Figure III-5 correspond to the maximum potential-drop observed during each substorm that occurred while Chatanika or Millstone were in the dawn or dusk sectors. The agreement with the satellite results is quite good.

A precise verification of our estimates of Φ can and will be done using radar data taken later when coincident DE passes occurred.

In summary, this first look at substorm convection signatures from three stations showed that:

- The substorm signature depends on the local time at which it is observed. The electric field appears to reverse when the station is near noon and midnight, and to intensify near dawn and dusk.
- In one case, an abrupt intensification of the electric field was observed simultaneously at two stations, one at dusk and one at dawn.
- An estimate of the cross polar-cap potential may be possible by doubling the auroral-zone potential measured from the incoherent-scatter electric field. The variations of Φ with the solar-wind ε parameter agree well with earlier satellite results.

With regard to the convection pattern signatures of a substorm, a major problem remains: determining whether an ion velocity enhancement or reversal is an actual change in the overall convection pattern, a rotation of the convection pattern, or an expansion of the preexisting pattern, or some combination of these factors.

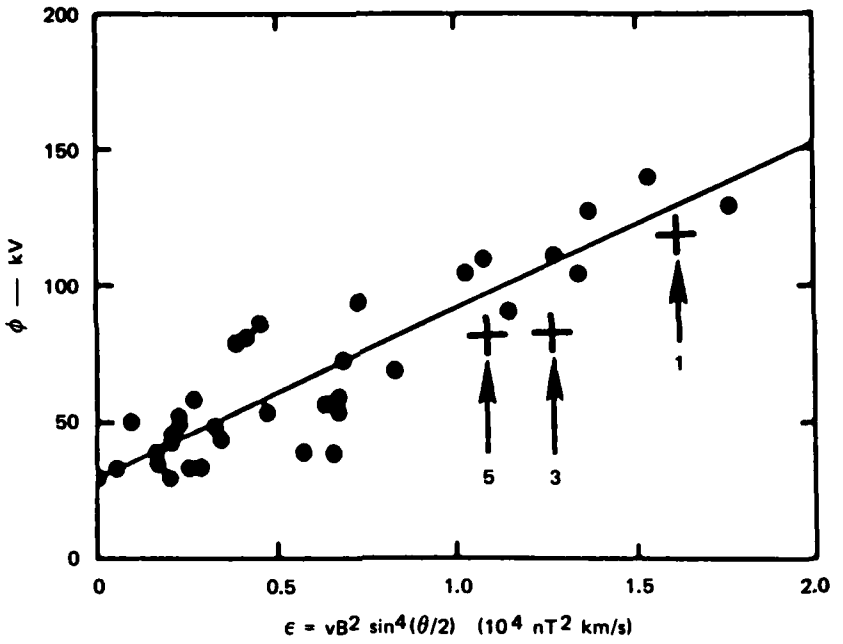

FIGURE III-5 CROSS POLAR CAP POTENTIAL VERSUS SOLAR-WIND ENERGY PARAMETER, ϵ [from Reiff et al., 1981]. The numbers on the figure refer to the substorms. Points # 1 and # 5 were in the dusk sector, measured by Chatanika and Millstone Hill, respectively. Point # 3 was in the dawn sector, measured by Chatanika.

2. Observations on 11 November 1981: Subauroral Electric Field

One of the most active MITHRAS days was 11 November 1981. Several substorms occurred on that day, and the IMF B_z component remained southward during more than seven hours. Some of the aspects of this day that are under investigation include: trough formation, F-region enhancements (blobs), IMF B_y influence on convection, substorm related convection, ring-current shielding, and subauroral electric fields. This last topic refers to electric fields equatorward of the region of auroral particle precipitation. Preliminary observations were briefly described by Senior (1982), in a study of Chatanika and Dynamics Explorer-B data. The Chatanika experimental mode was MITHRAS #3 (elevation scan). Figure

III-6 shows electron density contours in the meridian plane, and electrodynamic parameters (conductivities, electric field and electrojet current). The x and y axes are positive toward east and north, respectively. The subauroral electric field is clearly apparent on Figure III-6 in the region between Λ = 63 and 64° where the conductivities are very small. It is very intense (~ 50 mV/m) and as large as in the auroral zone. The relative positions of the equatorward boundaries of the diffuse aurora, electrojet, and electric field remained stable for several hours during this experiment. Preliminary DE data (R. Heelis, private communication) revealed that the equatorward edge of the downward field-aligned current coincided with the eastward electrojet equatorward edge, and that this limit is south of the plasma-sheet precipitation. Thus, the field-aligned currents flowed in the region of large subauroral electric field, in agreement with theoretical predictions of Vasyliunas (1972), and Pellat and Laval (1972). A theoretical model that describes the penetration of electric field to subauroral latitude is described later in this section. These observations of 11 November 1981 seem consistent with the model, but a detailed comparison between the model and the observations has not yet been done.

D. F-Region Morphology

Troughs in the auroral ionosphere have been observed in satellite and radar data since 1965 (Muldrew, 1965). One explanation for the appearance of these troughs is the stagnation theory (Knudsen, 1974; Spiro et al., 1978). According to this model, magnetic flux tubes are convected from the dayside to the nightside across the polar cap as a result of the magnetospheric electric field. These tubes return to the dayside by subsequently drifting westwards or eastwards. The westward convection velocity must be large enough to overcome the eastward corotation velocity if the plasma is to reemerge in sunlit regions. If not, the ionization falls to very low levels as it recombines. The trough is the locus of flux tubes that spend a long time in darkness because of the competing effects of the convection electric field and corotation.

The electron density results obtained with the MITHRAS and similar experiments show that when a trough does form, there is great variation

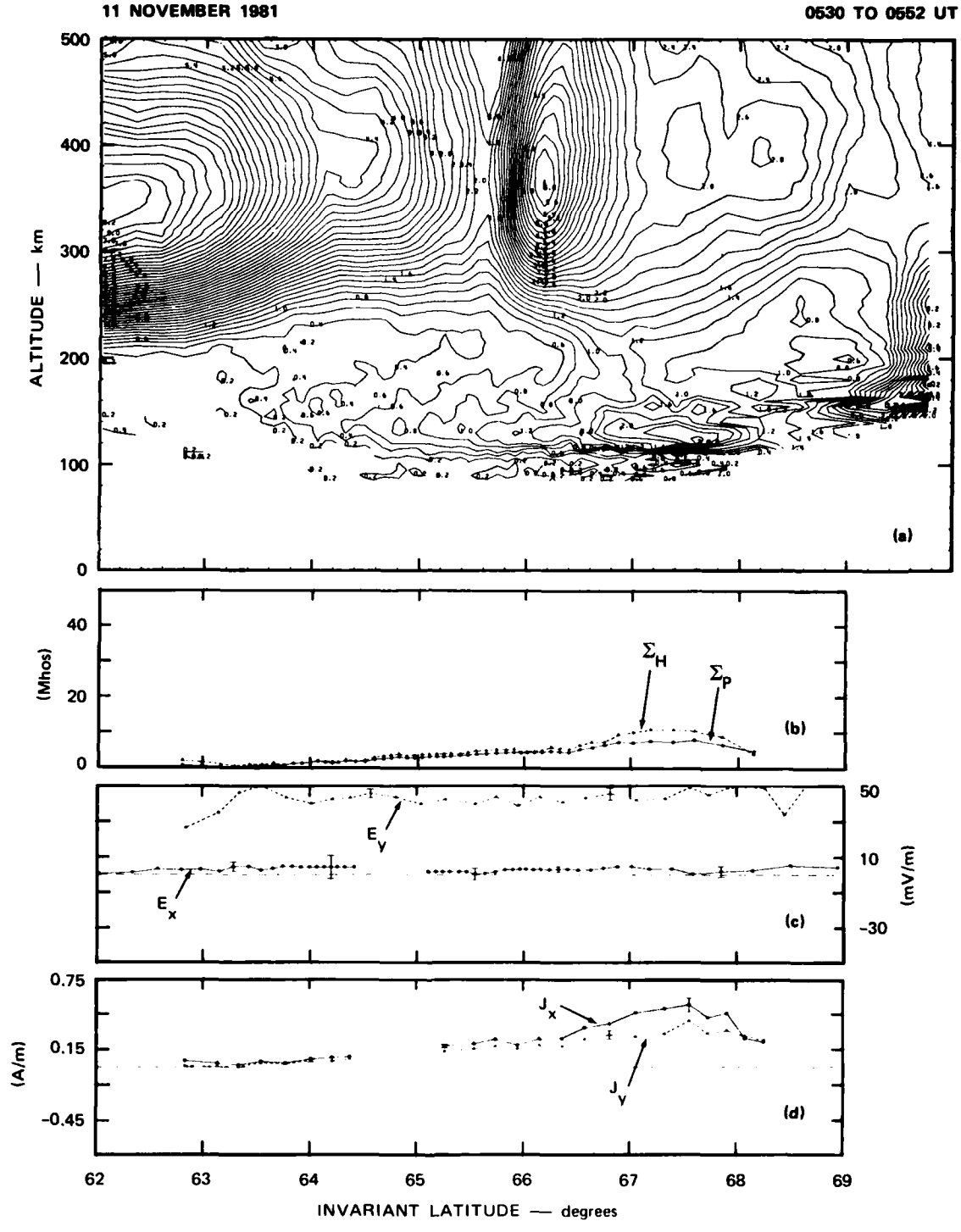

FIGURE III-6 PHYSICAL PARAMETERS ALONG THE CHATANIKA MAGNETIC MERIDIAN FOR 11 NOVEMBER 1981. Panel (a): Electron-density contours — the trough is visible 70 km north of Chatanika; Panel (b): Hall and Pedersen integrated conductivities; Panel (c): Eastward (solid line) and northward (dashed line) components of the electric field; Panel (d): Equatorward (solid line) and poleward (dashed line) components of the integrated current, perpendicular to the magnetic field.

in its location, duration, and time of appearance. On some nights, the trough does not form at all. Furthermore, the trough often seems to appear in regions in which the electric field is very large; the ion drift velocity often greatly exceeds the speed of the earth's rotation.

None of this behavior is entirely consistent with the stagnation theory of trough formation. An alternative explanation is that troughs are formed in regions of very strong convection (>1 km/s) as suggested by Schunk et al. (1976). Troughs that appear in the daytime have been observed associated with intense northward electric fields of magnetospheric origin. On the nightside, this mechanism can create multiple troughs in successive substorms. The troughs are subsequently observed to corotate towards dawn.

In addition to trough formation in the auroral zone, other features include regions of enhanced electron temperature that are sometimes seen equatorwards of the trough and presumably indicate L shells in which the plasmasphere and the ring current interact. Also, large daytime reductions in F-region density follow intense magnetic activity in summer and equinox. These low density regions extend as far equatorward as the Millstone Hill radar can see ($\Lambda \sim 40°$) and probably result from a reduction in the $(O)/(N_2)$ ratio because aurorally generated equatorward winds transport O to lower latitudes.

E. Empirical and Theoretical Modeling Efforts

1. Seasonal and Solar Cycle Variations

The results of a study of the seasonal and solar-cycle dependences of the ionosphere and thermosphere over Chatanika as deduced from 108 experiments spanning an 11-year period were reported by Baron et al. (1982) and Kelly et al. (1982). Data collected at Chatanika for the MITHRAS program were used for the last year of the 11-year period.

The study showed that the ionization maximum in the daytime solar-produced E-region depends on the square root of the 10.7-cm solar flux parameter and on $(\cos\chi)^{\gamma}$, where γ is approximately 0.7, and χ is the solar zenith angle.

The ionization in the F-region peak is given by

$$N_e \propto SA \times (\cos\chi)^{\frac{1+\Gamma}{2}} \qquad \text{(III-4)}$$

where

χ = solar zenith angle

SA = 10.7-cm solar flux parameter

Γ = scale-height gradient $\simeq$ 0.4.

This result is consistent with a Chapman Alpha production function, including a linear scale-height gradient.

In the F-region, the maximum ionization achieved during the day is a function of the 10.7-cm solar flux. In addition, there is a strong seasonal dependence with quite different behavior in the winter months as compared with the summer months. The switchover between summer and winter occurs very rapidly, within a week or so of equinox. In all the summer months, (April through September) the maximum density is proportional to the solar flux. In the winter months, the maximum density, $N_e(\max)$, is significantly greater than in summer, a manifestation of the "winter anomaly." $N_e(\max)$ in winter is not a linear function of the solar flux, but, rather, a quadratic function.

$$N_e(\max) = \begin{cases} (SA/100)\ 2.5 \times 10^5\ el/cm^3, & \text{--summer} \\ (SA/100)[2.5 + 0.05(SA - 60)] \times 10^5\ el/cm^3 & \text{--winter.} \end{cases} \qquad \text{(III-5)}$$

The agreement between the observed $N_e(\max)$ and the one calculated from Eq. (III-5) is quite good, as demonstrated by Figure III-7.

It is postulated that the rapid switchover between summer and winter conditions, and the higher wintertime densities are due to the change in meridional neutral thermospheric winds and the consequent modification of the ratio of atomic oxygen to molecular nitrogen. Roble

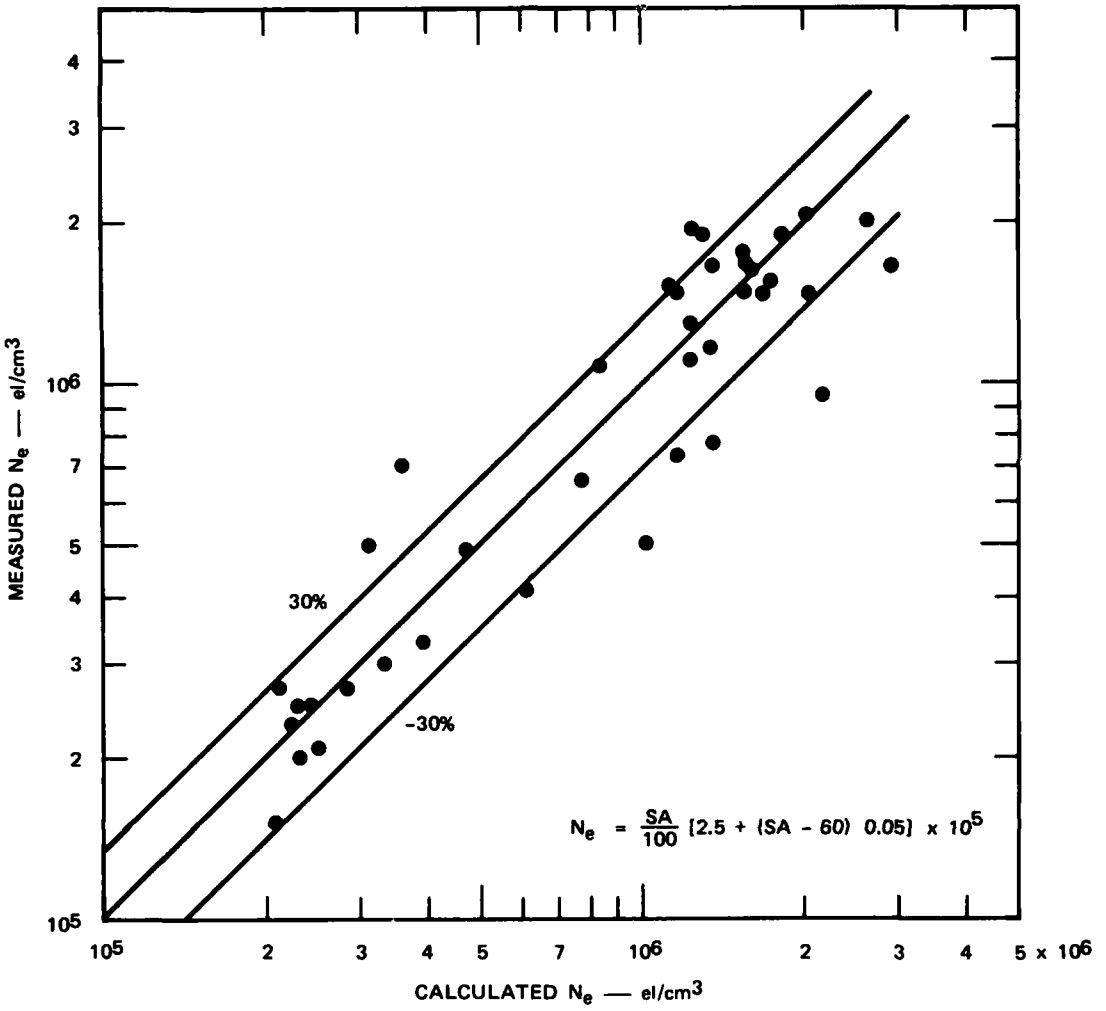

FIGURE III-7 A COMPARISON BETWEEN MEASURED AND CALCULATED [f(SA)] WINTER DAY F-LAYER MAXIMUM ELECTRON DENSITY

et al. (1977) modeled the mean thermospheric circulation. They find that a mean meridional circulation pattern exists in which the neutral gas rises in the summer hemisphere, flows horizontally toward the winter hemisphere and then descends. This gives rise to a horizontal transport of atomic oxygen. They also found that the equinox transition of the direction of the flow is very rapid; this finding is consistent with the rapid transition shown in Baron et al. (1982). This circulation pattern preferentially enhances the $(O)/(N_2)$ ratio in the winter hemisphere.

The inverse mechanism from that mentioned in the previous section is operative in winter, resulting in higher electron densities. In addition, the altitude of the layer maximum also depends on the $(O)/(N_2)$ ratio, consistent with the results stated in Baron et al. (1982).

The eleven years of data have also enabled an analysis of short, medium, and long term variations of exospheric temperature (Kelly et al., 1982). The diurnal variation seemed to vary between 100 and 300K, with the maximum during equinox at sunspot-maximum. Seasonal variations in the exospheric temperature were also examined. The maximum temperatures are in the summer, and the maximum variation is during sunspot maximum.

Finally, solar-cycle variations of exospheric temperature correlated quite well with SA values. The variation in the daily mean exospheric temperature from sunspot minimum to sunspot maximum was 600K.

2. Average Electric Fields

Work has started on an empirical model of the average electric fields at auroral latitudes. The model can be a function of K_p, IMF direction and season, and can also be extended to include other parameters. As a first step, Wand and Evans (1981a) reported average values of the southward and eastward electric-fields for Λ = 60°, 65°, 70°, and 75° based on all of the measurements obtained over May to December 1978 reported by Evans et al. (1980). Averages are now available for the entire data set gathered between June 1978 and August 1981, embracing, in all, 35 experiments, some of which were MITHRAS. Most lasted between 24 and 48 hours. The observed line-of-sight ion drift-velocities were sorted into 'bins' of ½-hour intervals (centered on the hour and half-hour of MLT at the observing point), and 2° intervals of Apex latitude (Apex latitude is very close to invariant latitude). This created a total of 432 'bins.' We then assumed that each of these cells had been viewed by the radar over a wide range of aspect angles during the 35 experiments so that the radial velocities could be averaged to secure the true mean drift velocity vector. The data were separated further into

three levels of K_p and according to whether the IMF was 'towards' or 'away' from the sun.

One example of this model is Figure III-8 which shows vectors representing the resulting drift velocities for active periods. This map and those generated for lower K_p show the expansion of the auroral oval with K_p. In all these average maps the convection reversal associated with the cusp always occurs before noon. It occurs later for IMF away (which usually corresponds to B_y positive, i.e. toward dusk). These average maps still suffer from the fact that they include data gathered over all seasons. Eventually, when enough data are available, it should be possible to produce separate maps for summer, winter, and equinox.

3. Conductivities

Ionospheric conductivities play an important role in the large-scale magnetosphere-ionosphere electrical circuit. For instance, when developing theoretical models, the global distributions of the currents that can be inferred from the electric field, and, conversely, the distribution of electric field that can be inferred from the current, are quite sensitive to the conductivity model used (Kamide and Richmond, 1982).

Work has started on an empirical model of conductivities based on the Chatanika data, which takes into consideration the role of both the solar EUV production and the production from energetic particles. Figure III-9 illustrates the conductivity variations with solar zenith angle for a period of two days in the summer. Both Σ_P AND Σ_H vary almost linearly with $\cos\chi$. Figure III-9 only contains the points calculated for the morning period. At midlatitude (Saint-Santin) the conductivities in the morning were found to be about 10% larger than in the afternoon, a difference attributed to variations in NO concentration (Senior et al., 1981). To determine if this asymmetry is present at a higher latitude, we plotted the morning and afternoon conductivities separately. A preliminary look at the Chatanika data did not seem to show any appreciable differences in the morning and afternoon conductivities, but clearly, more days need to be analyzed before any conclusion can be made.

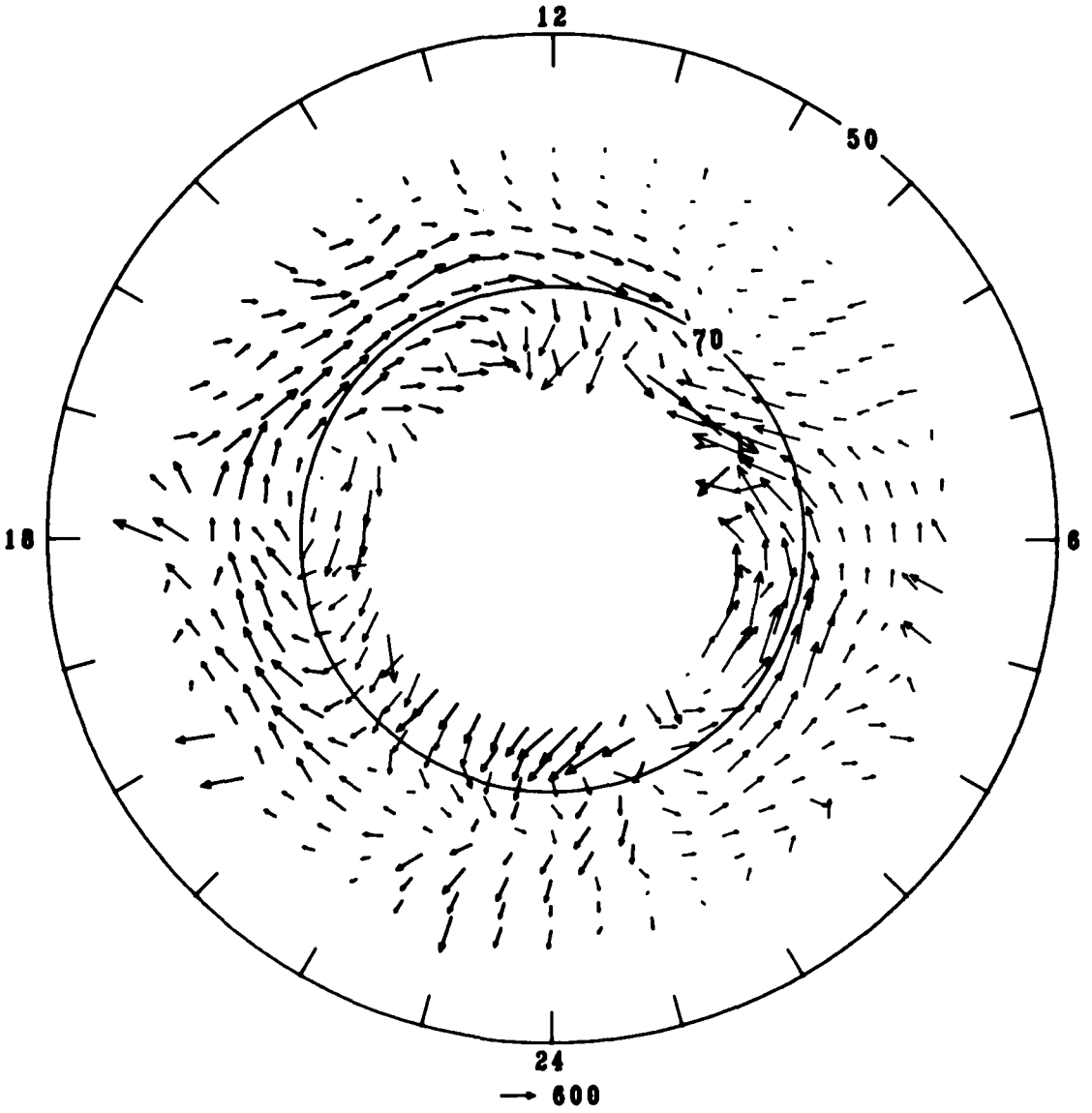

FIGURE III-8 AVERAGE DRIFTS OBSERVED FROM MILLSTONE HILL OVER TWO YEARS

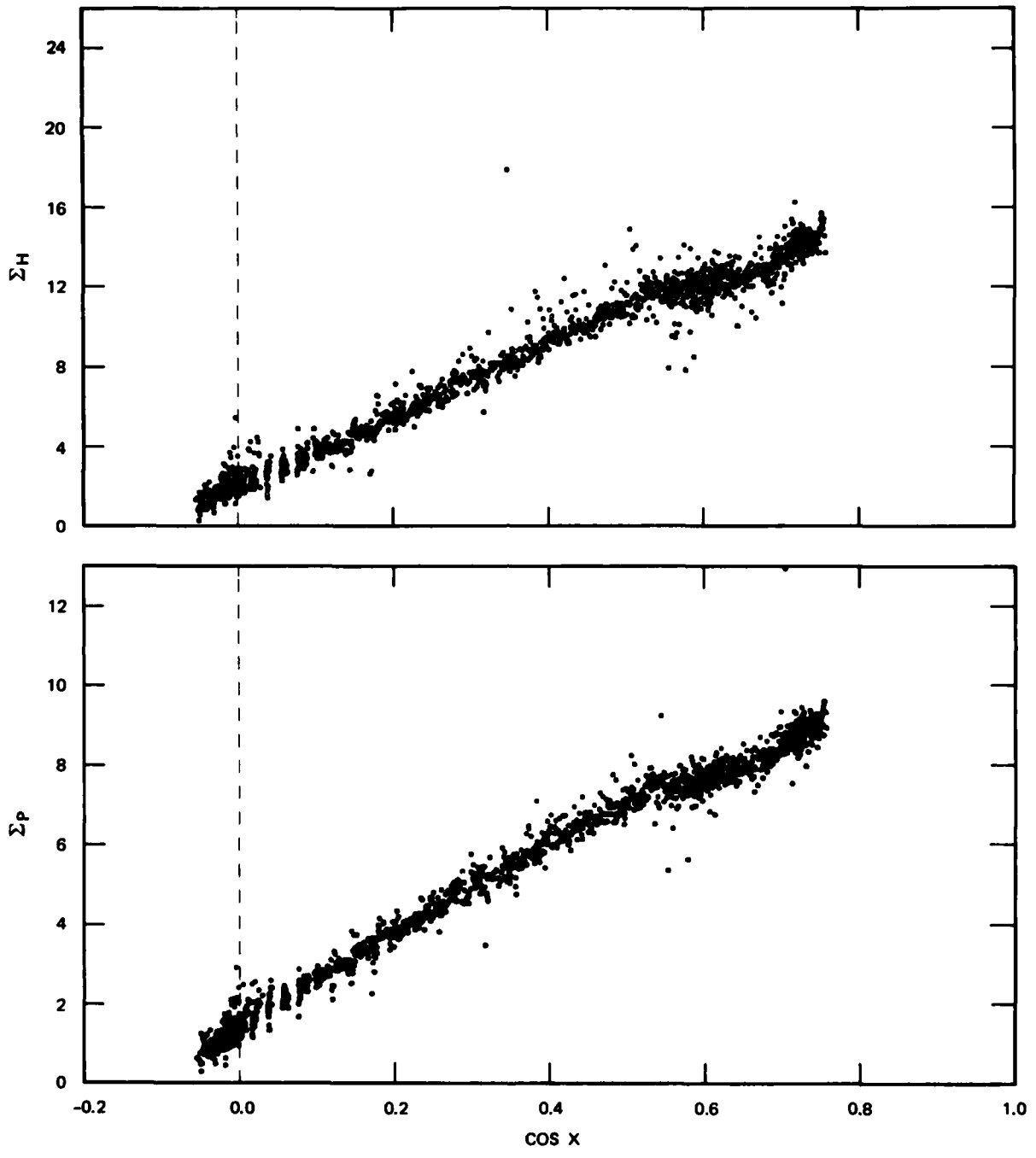

FIGURE III-9 SCATTER PLOT OF HALL AND PEDERSEN CONDUCTIVITIES AS A FUNCTION OF THE COSINE OF THE SOLAR ZENITH ANGLE. Only the morning points of the period from 10 to 11 June 1981 are included.

Work has also begun on an empirical model of the nighttime conductivities. The aim is to characterize the conductivities by a function of the total electron energy deposition and of the average energy of the incident flux (eleven such energy fluxes were considered). Figure III-10, for example, illustrates the relationship between conductivities and average energy for two values of the total energy flux. The solid curves also plotted on Figure III-10 represent the expected conductivities for incident electrons with a Maxwellian energy distribution (Vickrey et al., 1982). The agreement between the measured values and the theoretical values is fairly good, although the data points are systematically below

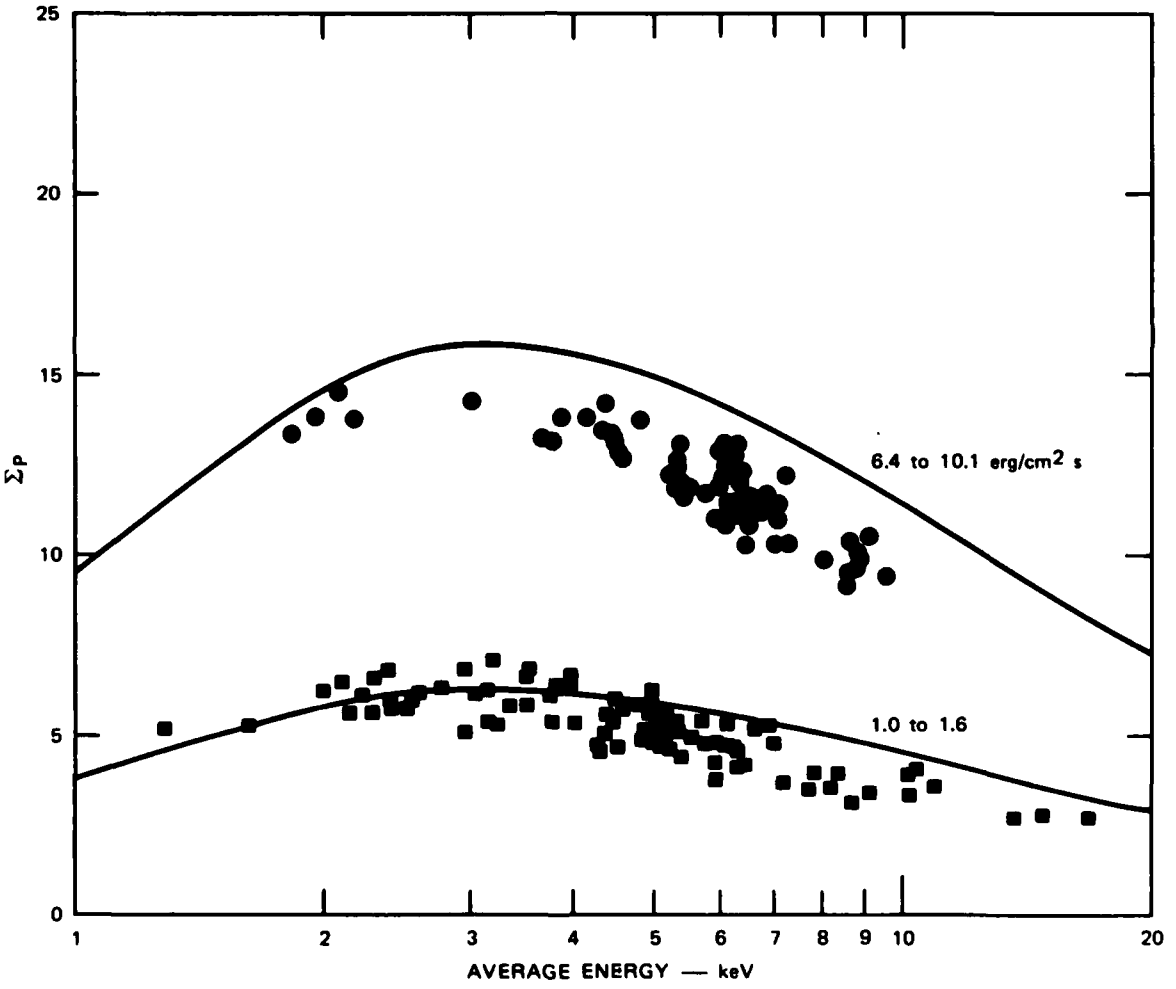

FIGURE III-10 SCATTER PLOT OF PEDERSEN CONDUCTIVITIES AS A FUNCTION OF AVERAGE ENERGY FOR TWO LEVELS OF TOTAL PRECIPITATED ENERGY. The solid curves represent the theoretical Σ_p calculated from an incident Maxwellian electron population.

values is fairly good, although the data points are systematically below the theoretical curve at high average-energies. The reason for this discrepancy is not clear at this point. Only one day's data are shown in Figure III-10. The analysis will encompass all the MITHRAS days and will eventually lead to empirical relationships for the conductivities that will be used in theoretical models.

4. Theoretical Modeling of Ring Current Shielding

While the above studies are concerned mostly with the auroral zone, this one is concerned with midlatitude convection electric fields which are associated with auroral activity. The question is whether a simple linear model of the convection can reproduce the latitudinal and local-time variations of the observed midlatitude disturbance electric field, E. A self-consistent, semianalystical, and time-dependent model has been developed of the ring-current coupling to the ionosphere via field-aligned currents. The model includes the reaction of the ring current to an externally imposed dawn-to-dusk potential drop across the magnetospheric cavity and the shielding of convection electric field from midlatitudes. This work is described in Senior and Blanc (1982).

In a first step, Senior and Blanc (1982) only introduced an auroral-zone conductivity enhancement between the polar-cap boundary and the equatorward boundary of the auroral zone, Λ_e. The boundary Λ_e is also the electron-precipitation boundary, it is distinct from, and generally poleward of Λ_i, the invariant latitude of the ring-current inner edge. Both Λ_i and Λ_e were taken as free parameters.

The equation of motion of the ring-current inner edge was related to the field-aligned currents, $j_{\parallel}$. These currents determine the distribution of the ionosphere potential Φ_i. The equation of charge conservation, combined with ionospheric Ohm's law gives:

$$\vec{\nabla} \begin{bmatrix} \Sigma_P & \Sigma_H \\ -\Sigma_H & \Sigma_P \end{bmatrix} \nabla\vec{\Phi}_I = -j_{\parallel} \sin I \qquad \text{(III-6)}$$

where

I = inclination of magnetic field.

The important aspect of this model is in the self-consistent, time-dependent calculation of $j_{\parallel}$. The analytical solution of this differential equation led to the following results:

(1) The enhancement of the auroral-zone conductivities reduces the effectiveness of the shielding of the convection electric field, both in terms of time constant and absolute amplitude of E.

(2) In the steady state, the spatial displacement between the ring-currents inner edge and the electron precipitation boundary generates intense electric fields in the subauroral zone. This result is illustrated in Figure III-11(a) where the electric field is plotted versus invariant latitude. The dashed curve represents E at the initial time, i.e. when the dawn-dusk potential in the magnetosphere increases as a step function, but when the midlatitude shielding of the convection electric field has not yet taken place. The solid line represents the steady state solution, which is reached within about one hour. The subauroral electric-fields are intensified by a decrease of either the subauroral conductivities, or of the latitudinal width of the auroral zone.

In a second step, Senior and Blanc (1982) included a realistic distribution of the midlatitude conductivities as a function of latitude and solar zenith angle. They derived the time-dependent response of the circuit to the step-function in the dawn-to-dusk potential. The initial-time and steady-state distributions of the ionospheric electric field compared rather well with the statistical models of the disturbance electric field presented by Blanc (1978) for the latitude of Saint-Santin, ($\Lambda = 44°$) and by Wand (1981) and Wand and Evans (1981a,b) for the latitude of Millstone Hill ($\Lambda = 56°$). This comparison with Millstone Hill is illustrated by Figure III-11(b) which shows the local-time distributions of the electric field-components deduced by the model. From this comparison and that at the Saint-Santin latitude, it was found that, in terms

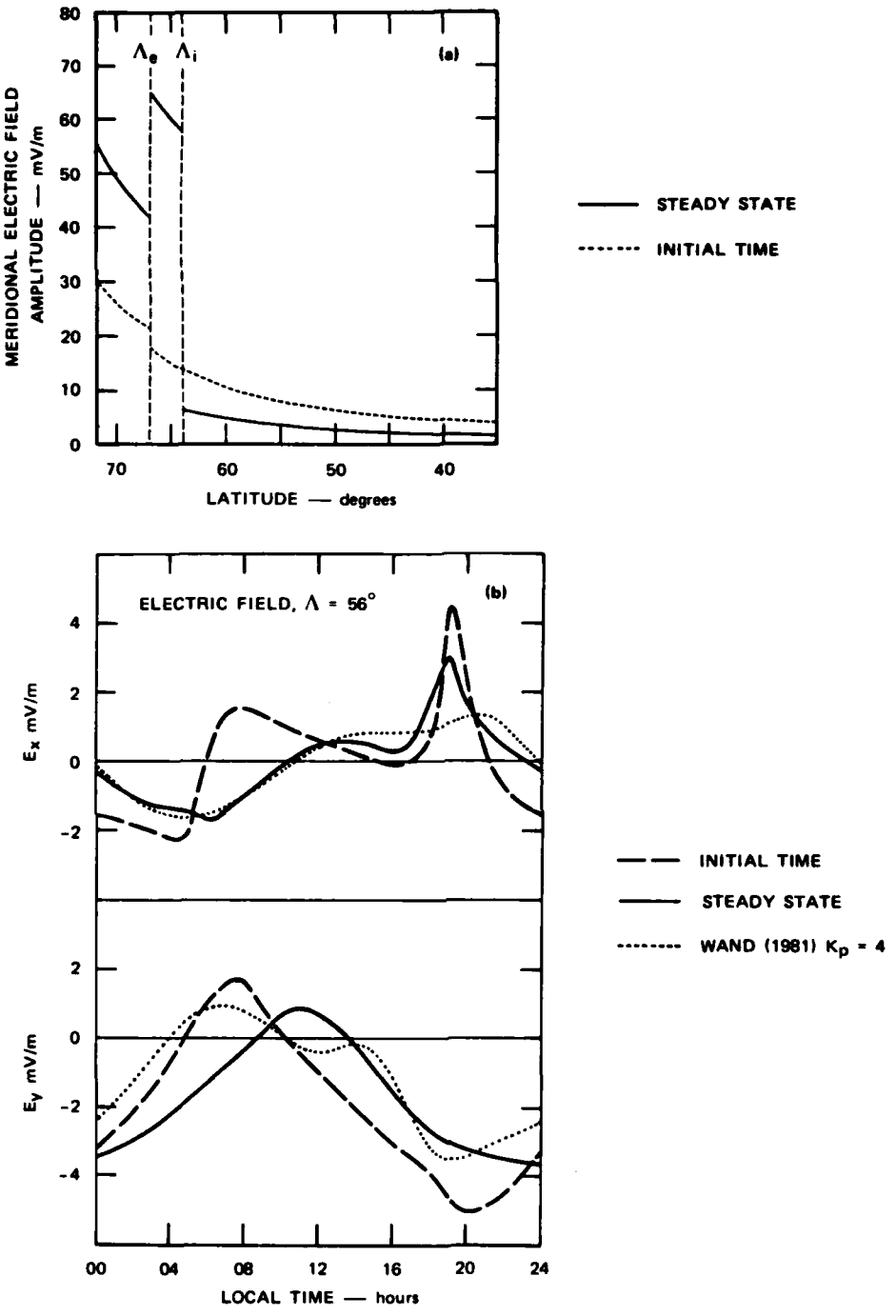

FIGURE III-11 FOR INITIAL TIME AND STEADY STATE, (a) LATITUDINAL PROFILE OF THE MERIDIONAL ELECTRIC-FIELD AMPLITUDE; (b) LOCAL-TIME VARIATION OF THE TWO COMPONENTS OF THE ELECTRIC FIELD PRODUCED AT $\Lambda = 56^\circ$ BY A 50-kV POTENTIAL DROP ACROSS THE POLAR CAP. The initial time amplitudes are divided by a factor of two to facilitate the comparison. The dotted curves represent Wand's [1981] model of the disturbance electric field over Millstone Hill for $K_p = 4$.

of absolute amplitude, the steady-state field is large enough to explain the statistical models.

This indicates that there is no basic failure in the concept of ring-current shielding, but that its efficiency to prevent magnetospheric convection electric-fields from penetrating to midlatitudes has probably been overestimated in the past. The overall consistency between the observations and the model is very promising and supports the idea that the linear theory can realistically reproduce the coupling between the ionosphere and the part of the magnetosphere where the magnetic field lines are closed.

IV INTERACTIONS

A. MITHRAS Meetings

Since MITHRAS is, by definition, a collaborative program, considerable attention has been given to interactions among the participants. In addition to informal contacts that take place continuously, two MITHRAS meetings were held. The first one was 27 January 1982 in Yosemite during the conference on "Origins of Plasmas and Electric Fields in the Magnetosphere." The MITHRAS meeting was attended by 16 people. The discussions dealt with the general research topics that could benefit from MITHRAS observations, the basic questions that should be asked, as well as the geophysical parameters and correlative measurements that would be needed.

It was also decided during the Yosemite conference that a MITHRAS working group should be formed. This group would be restricted to individuals directly interested in the MITHRAS data. It would be chaired by O. de la Beaujardiere of SRI International.

The first meeting of this MITHRAS working group was held at SRI on 23 and 24 August 1982. The specific aim was to compare DE and MITHRAS coincident data sets. Three active periods were selected for comparison: 25 October, 11 November, and 18 November 1981. For each period the most interesting aspects of the data were defined, and "subteams" were formed to work on them.

B. Data Exchange

A common format to represent the data is essential for comparisons. We devised a simple and flexible format that can be used to write incoherent-scatter parameters as well as parameters from other instruments such as STARE and DE. The same format is scheduled to be adopted by the incoherent-scatter community to archive the data in an NCAR data base.

The data are arranged into logical files that consist of a "prologue," or header, and a matrix of parameters. The size of both the prologue and and matrix can be varied from file to file.

It is neither convenient nor economical to have a unique file that contains all the parameters obtained from each experiment. The grids at which these parameters are measured vary from one data type to the next, and each data type is derived from a different analysis program. Furthermore, the most complicated analysis programs may not be routinely run for all the experiments, especially if funds and time are limited. Therefore, there are several data files for each MITHRAS experiment.

Since all the data are written in 16-bit integers (two's complement), most quantities are scaled by the appropriate factor before being written.

A precise description of the prologue is given in Tables IV-1 to 5. It contains basic elements such as time, coordinates, length of prologue, and dimension of the data matrix.

The data matrix itself has m columns and n rows where m is the number of parameters, and n is the number of ranges or heights at which the parameters were measured. As an illustration, Table IV-6 shows the arrangement of a data matrix for ACF data. As seen, the matrix actually has an extra row (row zero) which contains the codes to uniquely define the parameters present in the matrix. These data codes are listed in Table IV-5, along with the unit used, and the scaling factor. This factor is the number by which the value is multiplied before being written on tape. All error bars are coded by adding 100 to the parameter code. For example, 19 is the code for line-of-sight velocity, and 119 is the code for the statistical error in line-of-sight velocity. The largest possible error-bar value (i.e., 32767) indicates an aberrant point. A negative error bar indicates that the point has been manually edited out.

Several MITHRAS tapes have already been exchanged between participants. They are listed in Table IV-7.

Table IV-1

DATA RECORDS FORMAT

Number	Name	Element	Description
1	LTOT		Length of this record
2	KHD	h/d Code	Code to differentiate between header records and data records (1 and 2, respectively)
3	KRAD	Radar Code	Number to indicate from which radar this data comes (see Table IV-2)
4	KINDAT	Family Code	Number to indicate what kind of data is included (see Table IV-3)
5-8	ITIM	Date and Time	Field is four words long (see Table IV-4)
9-10	KOORD	Coordinate	Coordinates of point at which observation is performed (Either AZ, El x 10, or geographic latitude, longitude x 100, or geomagnetic)
11	KKOOR	C-code	Code to indicate whether coordinate system is polar, geographic, or geomagnetic (10, 20, and 30 respectively)
12	LPROL	l-Prologue	Length of prologue
13	MPAR	m	Number of different parameters
14	NROW	n	Number of different ranges (or heights)
———	———	———	Other items, if needed, to characterize parameters, or how they were obtained.
	KB	Data	Data matrix, m columns, n rows First row (row zero) contains codes to define parameters present (see Table IV-5)

Table IV-2

RADAR CODE

10	Jicamarca
20	Arecibo
30	Millstone Hill
40	Saint Santin
50	Chatanika
60	STARE
70	EISCAT(71, 72, 73 for Kiruna, Tromso, Sodankyla)
80	SRI Greenland radar

Table IV-3

CODE TO INDICATE KIND OF DATA

Number	Description
10 to 19	Basic, line of sight parameter. For Chatanika data, 10 is for PRISIS parameters (raw density, line of sight velocity), and 11 is for ACFIT parameters (temperatures, etc.)
20-29	Vector and electrodynamic parameters obtained from programs such as SATORI, EPEC, BLEDEN, etc.
30-39	Data from STARE

Table IV-4

DATE AND TIME FIELD

Number	Description	Example
1	Year	1981
2	Month and day (MMDD)	0825
3	Hours and minutes (HHMM)	1053
4	Seconds (ss)	37

Example is for 25 August 1981 at 1053:37 UT

Table IV-5

CODE TO UNIQUELY DESCRIBE PARAMETER

Code	Parameter	Unit	Factor
100	Range or alt. of autocorrelator gate	km	1
11	Ion temperature (Ti)	d K	1
12	Temperature ratio (Tr)	___	1000
13	Electron temperature (Te)	d K	1
14	Composition	%	1
19	Line of sight velocity (Vlos)	m/s	1
22	Chi square of fit	___	1000
23	Goodness	___	1
70	SNR	___	1000
72	Electron density (Ne)	el/cm**3[+]	0.001
74	Log, base 10, of el density	___	1000
1010	MAC Neutral wind, east (ux)	m/s	1
1011	MAC Neutral wind, north (uy)	m/s	1
1012	MAC Pedersen conductivity (σp)	mho/m	10**6
1013	MAC Hall conductivity (σh)	mho/m	10**6
1014	MAC Total current, east (jx)	A/m**3	10**8
1015	MAC Total current, north (jy)	A/m**3	10**8
1016	MAC Total joule heating (jH)	erg/s/cm**3	10**8
1017	Resolved velocity, east (Vx)	m/s	1
1018	Resolved velocity, north (Vy)	m/s	1
1019	Resolved velocity, parallel (V)	m/s	1
1020	OAC Neutral wind, east (Ux)	m/s	1
1021	OAC Neutral wind, north (Uy)	m/s	1
1022	Int. Ped. conductivity (Σp)	mhos	100
1023	Int. Hall conductivity (Σh)	mhos	100
1024	OAC Total current, east (Jx)	A/m	1000
1025	OAC Total current, north (Jy)	A/m	1000
1026	OAC Total joule heating (JH)	erg/s/cm**2	100
1027	Electric field, east (Ex)	mv/m	100
1028	Electric field, north (Ey)	mv/m	100
2011	Ion temperature, fit 2 (Ti2)	K	1
2012	Temperature ratio, fit 2 (Tr2)	___	1000
2013	Electron temperature, fit 2 (Te2)	K	1
2014	Composition, fit 2	%	1
2019	Line-of-sight velocity, fit 2 (Vlos 2)	m/s	1
2022	Chi square of fit 2	___	1000
2023	Goodness of fit 2	___	1
2072	Electron density, fit 2 (Ne2)	el/cm**3	0.001
2074	Log, base 10 of el density	___	1000
4000	MLT(1) year	year	1
4001	MLT(2) month and day	MMDD	1
4010	MLT(3) hours	hours	1000
5000	Invariant latitude	degrees	100

[+]The exponent follows a double asterix

Table IV-6

THE DATA MATRIX

Parameter	P1	P2	P3	P4	P5	P6	P7
Height 1	r_1	Te_1	ΔTe_1	Ti_1	ΔTi_1	Ne_1	ΔNe_1
Height 2	r_2	Te_2	ΔTe_2	Ti_2	ΔTi_2	Ne_2	ΔNe_2
Height n	r_n	Te_n	ΔTe_n	Ti_n	ΔTi_n	Ne_n	ΔNe_n

Table IV-7(a)

EXCHANGE OF MITHRAS TAPES

Tapes of Chatanika Data Mailed out by SRI					
Data Date (1981)	Data Description	MITHRAS #	Radar	Mailed to	Date Mailed (1981)
27 June	N_e, T_i, T_e along line of sight (OAC)	1	Chatanika	Holt	5 March
30 Sept	V_i, T_i, T_e along line of sight (OAC)	2	Chatanika	Alcayde	10 March
27 June	Raw CHATOL tape	1	Chatanika	Foster	13 March
02 Aug	Raw CHATOL tape	1	Chatanika	Foster	15 March
30 Sept	Electrodynamic parameters (OAC)	2	Chatanika	Alcayde	26 March
30 Sept	N_e, T_i, T_e along line of sight (MAC)	2	Chatanika	Roble	30 March
30 Sept	Electrodynamic parameters (MAC)	2	Chatanika	Roble	31 March
18 Nov	N_e, T_i, T_e along line of sight (OAC)	2	Chatanika	Alcayde	5 April
18 Nov	Electrodynamic parameters (OAC)	2	Chatanika	Alcayde	5 April

Table IV-7(b)

Tapes Received at SRI					
Data Date (1981-82)	Data Description	MITHRAS #	Radar	Mailed to	Date Received (1981)
27 June	N_e, T_i, T_e along line of sight	1	MH	de la Beaujardiere	1 April
27 June	Vx, Vy geographic coordinates	1	STARE	de la Beaujardiere	8 April
30 Sept	N_e, T_i, T_e, V_i along line of sight	2	EISCAT	de la Beaujardiere	10 July
18 Nov	N_e, T_i, T_e, V_i along line of sight	2	EISCAT	de la Beaujardiere	10 July
8 Dec	N_e, T_i, T_e, V_i along line of sight	3	EISCAT	de la Beaujardiere	10 July
27 Jan	N_e, T_i, T_e, V_i along line of sight	3	EISCAT	de la Beaujardiere	10 July
31 Jan	N_e, T_i, T_e, V_i along line of sight	1	EISCAT	de la Beaujardiere	10 July

C. Work in Progress With Other Groups

Collaborative work with scientists in the community other than those directly involved in gathering the MITHRAS data has just begun.

With S. Akasofu and coworkers, we have decided to select one MITHRAS day for in-depth analysis. This day should have well-defined substorms, and available magnetometer data from a large number of stations. The purpose is to run, for the selected period, the large global electrodynamic codes such as the KRM code (Kamide et al., 1981). Basically, these codes solve Eq. III-6 to derive the electric field distribution. This distribution will then be compared with the actual fields measured by the MITHRAS radars. The purpose of the comparison will be to refine the codes and to give a better understanding of the substorm effects.

R. Roble's interest is in the modeling of the E- and F-region winds. A tape was mailed to him with wind and electrodynamic parameters measured by the Chatanika radar during an active period (18 November 1981).

The work with R. Schunk will start by a comparison of his convection model with the actual convections measured by MITHRAS. A second step will be to compare his predicted ionospheric parameters with those of MITHRAS.

The collaboration with the DE team will start with a study of the convection pattern. R. Heelis plans to combine potential curves from the three radars and the DE-B satellite, at fixed UT, and determine the overall convection that best matches the observations. The period selected is 25-26 October 1971, when several DE passes were recorded.

Work has started with R. Clauer on the study of substorm electric fields and currents. The first day selected is 11 November 1981. The purpose is to analyze ground magnetometer data from high and midlatitude stations, along with radar, DE, and ISEE measurements, to see if it is possible to distinguish a separate current, the substorm electrojet, and the convection that would be associated with it.

V CONCLUSIONS

An intensive campaign of coordinated incoherent-scatter radar experiments took place in 1981-1982. It was planned to take advantage of the short period during which three incoherent-scatter radars could probe the auroral zone simultaneously. The three incoherent-scatter radars that participated in the MITHRAS experiments were Chatanika (Alaska), Millstone-Hill (Massachusetts), and EISCAT (Scandinavia). Collaborative studies were undertaken using data from the DE spacecraft and the STARE radar. The experimental modes were derived collaboratively among Millstone, Chatanika, and EISCAT scientists. There were three main types of MITHRAS experiments, each with a different scientific purpose. MITHRAS #1 was aimed at large latitudinal coverage of F-region drifts, electron-densities, and temperatures. MITHRAS #2 was designed for very good height and time resolution. MITHRAS #3 was intermediate between the other two modes. It provided both E- and F-region coverage over several degrees in latitude.

Under the MITHRAS project, substantial changes and additions were made to the software and hardware systems at Millstone and Chatanika.

Thirty-three MITHRAS experiments were performed. Most of the data have been reduced. The analysis and interpretation of the data are well underway. Among the scientific accomplishments we cite:

(1) Ionosphere--Ionospheric densities and temperature were compared for the three radars for selected periods and between the radar and the RADC model. A study of Joule heating in the F region revealed the importance of the electron density in ion drag and in neutral-wind morphology.

(2) Thermosphere--A method was developed to determine the auroral zone altitude profiles of neutral parameters such as temperature and oxygen concentration. Thermospheric parameters were obtained for several periods, and the EISCAT and Chatanika values compared.

(3) Magnetosphere--Detailed case studies dealt with the effect of substorms on convection. A three-radar comparison of the substorm signature in the electric field revealed that the signature depends primarily on the local time where the observation is made. The cross-polar cap potential was estimated from radar electric fields in the dawn or dusk sectors. Intense electric fields associated with substorms can be a predominant factor in the formation of ionospheric troughs. Subauroral electric fields were observed during a period of prolonged magnetic activity (11 November 1981), and interpreted in terms of ring-current shielding.

(4) Empirical Models--Models were constructed to characterize the day and night conductivities, the electric fields, the E- and F-region densities, and the exospheric temperature. These models yield averaged values of the observed radar parameters as a function of quantities such as K_p, solar flux, IMF, solar zenith angle, or precipitation.

(5) Theoretical Model--A theoretical model of the temporal variation and global effects of ring-current shielding was developed.

Scientific collaborations between the various groups took place informally and during MITHRAS working meetings. A number of data tapes were exchanged among groups. This exchange of data was facilitated by the implementation of a general data format.

Related to MITHRAS, there were 12 scientific publications, and 14 papers presented at international conferences.

IV REFERENCES

Alcaydé, D., and P. Bauer, "Modelisation des Concentrations d'Oxygène Atomique Observées par Diffusion Incohérente," Ann. Geophys., 33, 305, 1977.

Alcaydé, D., J. Fontanari, and P. Bauer, "High Latitude Neutral Temperature and Concentration Measurements from the First EISCAT Incoherent-Scatter Observations," Annales d'Astrophy., in press, 1982a.

Alcaydé, D., J. Fontanari, P. Bauer, and O. de la Beaujardière, "Some Properties of the Auroral Thermosphere Inferred from Initial EISCAT Observations," submitted to Radio Sci., 1982b.

Bauer, P., P. Waldteufel, and D. Alcaydé, "Diurnal Variations of the Atomic Oxygen Density and Temperature Determined from Incoherent-Scatter Measurements in the Ionospheric F Region," J. Geophys. Res., 75, 4825, 1970.

Baron, M. J., and A. R. Hessing, "Comment on 'A Simple Method for Calculating the Local Time of Corrected Geomagnetic Midnight,' by L. E. Montbriand," to be submitted to J. Geophys. Res., 1982.

Baron, M. J., and R. H. Wand, "F-Region Ion Temperature Enhancements Resulting from Joule Heating," Geophys. Res. Lett., in press, 1982.

Baron, M. J., C. J. Heinselman, and J. Petriceks, "Solar Cycle and Seasonal Variations of the Ionosphere Observed with the Chatanika Incoherent-Scatter Radar," submitted to Radio Sci., 1982.

Blanc, M., "Midlatitude Convection Electric Fields and Their Relation to Ring-Current Development," Geophys. Res. Lett., 5, 203, 1978.

de la Beaujardière, O., J. Holt and E. Nielsen, "Early MITHRAS Results: The Electric-Field Response to Substorms," submitted to Radio Sci., 1982.

de la Beaujardière, O., R. Vondrak, and M. Baron, "Radar Observations of Electric Fields and Currents Associated with Auroral Arcs," J. Geophys. Res., 82, 5051, 1977.

de la Beaujardière, O., V. Wickwar, C. Leger, M. McCready, and M. Baron, "The Software System for the Chatanika Incoherent-Scatter Radar," Technical Report, NSF Grant ATM 782358, SRI Project 8358, SRI International, Menlo Park, CA (November 1980).

Elkins, T. J., "An Empirical Model of the Polar Ionosphere," AFCRL-TR-73-0331, Air Force Cambridge Research Laboratories, Hanscom Field, Bedford, Massachusetts, 23 May 1973.

Evans, J. V., J. M. Holt, W. L. Oliver, and R. H. Wand, "Millstone Hill Observations of Auroral Convection Over $60° < \Lambda \leq 75°$, 2. Initial Results," J. Geophys. Res., 85, 41, 1980.

Feldstein, Y. I., and G. V. Starkov, "Auroral Oval in the IGY and IQSY Period and a Ring Current in the Magnetosphere," Planet. Space Sci., 16, 129, 1968.

Folkestad, K., T. Hagfors, and S. Westerlund, "EISCAT--An Updated Description of Technical Characteristics and Operational Capabilities," submitted to Radio Sci., 1982.

Greenwald, R. A., W. Weiss, E. Nielsen, and N. R. Thomson, "STARE: A New Radar Auroral Backscatter Experiment in Northern Scandinavia," Radio Sci., 13, 1021, 1978.

Hedin, A. A., C. A. Reber, N. W. Spencer, H. C. Brinton, and D. C. Kayser, "Global Model of Longitude/UT Variations in Thermospheric Composition and Temperature Based on Mass Spectrometer Data," J. Geophys. Res., 84, 1, 1979.

Kamide, Y. and A. D. Richmond, "Ionospheric Conductivity Dependence of Electric Fields and Currents Estimated from Ground Magnetic Observations," J. Geophys. Res., 87, 8331, 1982.

Kelly, J. D., C. J. Heinselman, and J. Petriceks, "High-Latitude Exospheric Temperature Observed over a Solar Cycle," submitted to Radio Sci., 1982.

Knudsen, W. C., "Magnetospheric Convection and the High-Latitude F_2 Ionosphere," J. Geophys. Res., 79, 1046, 1974.

Leadabrand, R. L., M. J. Baron, J. Petriceks, and H. F. Bates, "Chatanika, Alaska, Auroral-Zone Incoherent-Scatter Facility," Radio Sci., 7, 747, 1972.

Montbriand, L. E., "A Simple Method for Calculating the Local Time of Corrected Geomagnetic Midnight," J. Geophys. Res., 75, 5634, 1970.

REFERENCES (Continued)

Muldrew, D. B., "E-Layer Ionization Troughs Deduced from Alouette Data," J. Geophys. Res., 70, 2635, 1965.

Pellat, R., and G. Laval, "Remarks on the steady and time-dependent mathematical convection models," in Critical Problems of Magnetospheric Physics, edited by E. R. Dyer, I.U.C.S.T.P., Washington, D.C., 1972.

Perreault, P., and S. -I. Akasofu, "A Study of Geomagnetic Storms," Geophys. J. R. Astron. Soc., 54, 547, 1978.

Reiff, P. H., R. W. Spiro, and T. W. Hill, "Dependence of Polar Cap Potential Drop on Interplanetary Parameters," J. Geophys. Res., 86, 7639, 1981.

Roble, R. G., R. E. Dickinson, and E. C. Ridley, "Seasonal and Solar Cycle Variations of the Zonal Mean Circulation in the Thermosphere," J. Geophys. Res., 82, 5493, 1977.

Senior, C., "Les Conductiviteés Ionosphériques et Leur Rôle dans la Convection Magnétospherique: Une Étude Expérimentale et Théorique," Thèse de 3ème cycle, Université de Paris, 1980.

Senior, C., "Courants Alignés, Prècipitations Diffuses et Électrojets dans le Secteur Nuit de Haute Latitude," Proceedings of GRECO Conference, Grenoble, France (September 1982).

Senior, C., P. Bauer, C. Taieb, and Michel Petit, "Le Rôle de L'Oxyde d'Azote dans la Distribution de Densité Électronique de la Region E en Fonction de L'angle Zénithal Solaire, C. R. Acad. Sci. Paris, 292, 1195, 1981.

Senior, C., and M. Blanc, "On the Control of Magnetospheric Convection by the Spatial Distribution of Ionospheric Conductivities," submitted to J. Geophys. Res., 1982.

Schunk, R. W., P. M. Banks, and W. J. Raitt, "Effects of Electric Fields and Other Processes Upon the Nighttime High-Latitude F Layer," J. Geophys. Res., 81, 3271, 1976.

Spiro, R. W., R. A. Heelis, and W. B. Hanson, "Ion Convection and the Formation of the Mid-Latitude F Region Ionization Trough," J. Geophys. Res., 83, 4255, 1978.

Vasyliunas, V. M., "The Interrelationship of Magnetospheric Processes," p. 29 in Earth's Magnetospheric Processes, edited by B. M. McCormac 1972.

Vickrey, J. F., R. R. Vondrak, and S. J. Matthews, "Energy Deposition by Precipitating Particles and Joule Dissipation in the Auroral Ionosphere," J. Geophys. Res., 87, 5184, 1982.

Vondrak, R. R., G. Smith, V. E. Hatfield, R. T. Tsunoda, V. R. Frank, and P. D. Perreault, "Chatanika Model of the High-Latitude Ionosphere for Application to HF Propagation Prediction," RADC-TR 78 7, 1978.

Wand, R. H., "A Model Representation of the Ionospheric Electric Field over Millstone Hill (Λ = 56°)," J. Geophys. Res., 86, 5801, 1981.

Wand, R. H., and Evans, J. V., "The Penetration of Convection Electric Fields to the Latitude of Millstone Hill (Λ = 56°)," J. Geophys. Res., 86, 5809, 1981a.

Wand, R. H., and Evans, J. V., "Seasonal and Magnetic Activity Variations of Ionospheric Electric Fields over Millstone Hill," J. Geophys. Res., 86, 103, 1981b.

Wickwar, V. B., "Chatanika Radar Measurements," Atmospheres of Earth and the Planets, pp. 111-124, B. M. McCormac, ed. (D. Reidel Publishing Company, Dordrecht-Holland, 1975).

APPENDIX A

Radar Operating Modes

The detailed operating modes for each of the three incoherent-scatter radars is given in Tables A-1, A-2, and A-3. These modes were used whenever possible but there were times when technical difficulties forced us to adopt a different mode. The three MITHRAS experiments objectives are described in Section II-B of this report.

Table A-1

CHATANIKA OPERATING MODES

Antenna	Invariant Latitude Coverage for E Field (deg)	Pulse Length	Cycle Time (min)
• Experiment 1--eleven discrete positions - 1 parallel to B - 5 pairs symmetrically placed with respect to magnetic meridian - 1 elevation scan in magnetic meridian every 5 complete cycles	58 to 75	400 μs (60 km)	30
• Experiment 2--three discrete positions - 1 parallel to B - 2 others ±60° from magnetic meridian at 70° elevation	65 to 66	60 μs (9 km) 320 μs (48 km) 3 × 60 μs (9 km)	10
• Experiment 3--elevation scan in magnetic meridian from 15°N elevation to 25°S elevation, plus partial scan along a meridian line displaced to west	63 to 68.5	60 μs (9 km) 320 μs (18 km)	20

Table A-2

MILLSTONE HILL OPERATING MODES

Antenna	Invariant Latitude Coverage for E Fields (deg)	Pulse Length	Cycle Time (min)
Experiment 1--350° azimuth scan at 4° elevation, scan rate 10°/min, vertical beam during retrace of steerable antenna. Beginning January 1982 also a 162° elevation scan.	38 to 75	2.0 ms (300 km) [0.64 ms (96 km) used on a few experiments]	40
Experiment 2--(a) 342° azimuth: 2°, 4°, 6° elevations for 30 s each position, 7° to 17° elevation scan taking 150 s; (b) 11° azimuth: 17° to 7° elevation scan taking 150 s, 6°, 4°, 2° elevations for 30 s each position.	61 to 72	Fixed positions: 0.64 ms (96 km) Scans: 1.28 ms (192 km)	11
Experiment 3--180° azimuth scan from east through north to west at 4° elevation, scan rate 10°/min. Vertical beam during retrace of steerable antenna	55 to 75	June to August: 1 ms (150 km) September onward: 1.28 ms (192 km)	21

Table A-3

EISCAT OPERATING MODES

Mode*	Antennas	Invariant Latitude Coverage for E Fields (deg)	Pulse Lengths	Cycle Time (min)
CP(0)	Tromsø: parallel to $\bar{B}$ Kiruna/Sodankyla: intersecting Tromsø beam at the 110-, 120-, 130-, 140-, 300-, and 700-km altitudes	66.4	500 μs (75 km)	~5
CP(-1)	Tromsø: parallel to $\bar{B}$ Kiruna/Sodankyla: intersecting Tromsø beam at the 300-km altitude	66.4	60 μs (9 km) for power profile and 360 μs (54 km) ACFs	~1
CP(-2)	Tromsø: three-beam directions forming a right-triangle Kiruna/Sodankyla: intersecting Tromsø beam at the 300-km altitude	65.5 to 67.2	60 μs (9 km) for power profile and 360 μs (54 km) for ACFs	6
CP(-3s)	Tromsø: three-beam directions in meridian plane Kiruna/Sodankyla: intersecting Tromsø beam at the 300-km altitude	65.5 to 67.2	60 μs (9 km) for power profile 360 μs (54 km) for ACFs	6
CP(-3e)	Tromsø: 11-beam directions in meridian plane Kiruna/Sodankyla: intersecting Tromsø beam at the 325-km altitude	64 to 69	60 μs (9 km) for power profile 320 μs (48 km) for ACFs 1000 μs (150 km) for remote stations	20
CP(3)	Tromsø: 16-beam directions in meridian plane Kiruna/Sodankyla: intersecting Tromsø beam at the 325-km altitude	61.3 to 71.3	60 μs (9 km) for power profile 360 μs (54 km) for ACFs 1000 μs (150 km) for remote stations	30

*CP designates "Common Program," i.e., data available to all EISCAT member countries, and, by agreement, also available to the MITHRAS program on an exchange basis.

APPENDIX B

LIST OF PAPERS AND ORAL PRESENTATIONS ON MITHRAS-RELATED WORK

MITHRAS Publication List

"Chatanika Radar Observations Associated with the MITHRAS Program," O. de la Beaujardiere, M. Baron, C. Senior, J. Petriceks, and C. Leger, Proceedings of the 1982 Yosemite Conference on the Origins of Plasmas and Electric Fields in the Magnetosphere, (1982).

"F-Region Ion Temperature Enhancements Resulting from Joule Heating," M. J. Baron and R. H. Wand, Geophys. Res. Lett., in press (1982).

"Some Properties of the Auroral Thermosphere Inferred from Initial EISCAT Observations," D. Alcayde, J. Fontanari, P. Bauer, O. de la Beaujardiere, submitted to Radio Sci. (1982).

"Solar Cycle and Seasonal Variations of the Ionosphere Observed with the Chatanika Incoherent Scatter Radar," M.J. Baron, C. J. Heinselman, and J. Petriceks, submitted to Radio Sci. (1982).

"Early MITHRAS Results: "The Electric-Field Response to Substorms," O. de la Beaujardiere, J. Holt, and E. Nielsen, submitted to Radio Sci. (1982).

"Millstone Hill Studies of the Trough: Boundary Between the Plasmapause and Magnetosphere or Not?" J. M. Holt, J. V. Evans, and R. H. Wand, submitted to Radio Sci. (1982).

"High-Latitude Exospheric Temperature Observed Over a Solar Cycle," J. D. Kelly, C. J. Heinselman, and J. Petriceks, submitted to Radio Sci. (1982).

"Comment on 'A Simple Method for Calculating the Local Time of Corrected Geomagnetic Midnight,' by L. E. Monbriant," M. J. Baron and A. R. Hessing, to be submitted to J. Geophys. Res. (1982).

"Measures Simultanées des Champs Electriques de l'Ionosphere Aurorale par les Radars d'EISCAT et de Chatanika," G. Caudal, D. Alcayde, O. de la Beaujardiere, and G. Lejeune, Proceedings of GRECO Conference, Grenoble, 1982.

"Courants Alignés, Precipitations Diffuses et Electrojets dans le Secteur Nuit de Haute Latitude," C. Senior, Proceedings of GRECO Conference, Grenoble, 1982.

"On the Control of Magnetospheric Convection by the Spatial Distribution of Ionospheric Conductivities," C. Senior and M. Blanc, submitted to J. Geophys. Res. (1982).

APPENDIX B (continued)

MITHRAS-Related Presentations to National or International Symposia

"Chatanika Radar Observations Associated with the MITHRAS Program," O. de la Beaujardiere, M. Baron, C. Senior, J. Petriceks, and C. Leger. Conference on the Origins of Plasmas and Electric Fields in the Magnetosphere, Yosemite, California, January 1982.

"Substorm Effects on Auroral Convection as Observed by the Millstone Hill Radar," J. M. Holt, J. V. Evans, and R. H. Wand, Conference on the Origins of Plasmas and Fields in the Magnetosphere, Yosemite, California, January 1982.

"High-Latitude Electric Fields Observed From Millstone Hill," J. V. Evans, R. H. Wand, J. M. Holt, and W. L. Oliver, Solar-Terrestrial Physics Symposium, Ottawa, Canada, May 1982.

"Millstone Hill Studies of the High-Latitude Ionosphere," R. H. Wand, J. M. Holt, J. V. Evans, and W. L. Oliver, Solar-Terrestrial Physics Symposium, Ottawa, Canada, May 1982.

"Simultaneous Measurements of the Electrodynamic Parameters of the Auroral Ionosphere by the EISCAT and Chatanika Radars," G. Caudal, D. Alcayde, O. de la Beaujardiere, and G. Lejeune, EGS Symposium, Leeds, UK, August 1982.

"High Latitude Neutral Atmosphere Temperature and Concentration Measurements From the First EISCAT Incoherent Scatter Observations," D. Alcayde, J. Fontanari, and P. Bauer, URSI Symposium, Fairbanks, Alaska, August 1982.

"Solar Cycle Variations of the High Latitude Ionosphere as Observed With Incoherent Scatter Radar," M. J. Baron, C. J. Heinselman, and J. Petriceks, URSI Symposium, Fairbanks, Alaska, August 1982.

"High-Latitude Exospheric Temperature Observed over a Solar Cycle," J. D. Kelly, C. J. Heinselman, and J. Petriceks, URSI Symposium, Fairbanks, Alaska, August 1982.

"Millstone Hill Observations of the Trough: Boundary Between The Plasmapause and Magnetosphere or Not?" J. M. Holt, J. V. Evans, and R. H. Wand, URSI Symposium, Fairbanks, Alaska, August 1982.

"Early MITHRAS Results: The Electric-Field Response to Substorms," O. de la Beaujardiere, J. Holt, and E. Nielsen, URSI Symposium, Fairbanks, Alaska, August 1982.

"F-Region Ion Temperature Enhancements Resulting From Joule Heating," M. J. Baron, URSI Symposium, Fairbanks, Alaska, August 1982.

"F-Region Plasma Enhancements Along the Equatorward Boundary of the Auroral Oval," R. T. Tsunoda, R. M. Robinson, and C. Senior, URSI Symposium, Fairbanks, Alaska, August 1982.

"Mesures Simultanées des Champs Electriques de l'Ionosphere Aurorale par les Radars d'EISCAT et de Chatanika," G. Caudal, D. Alcayde, O. de la Beaujardiere, G. Lejeune, GRECO Conference on Incoherent Scatter Observations, Grenoble, France, September 1982.

"Courants Alignés, Precipitations Diffuses et Electrojets dans le Secteur Nuit de Haute Latitude," GRECO Conference on Incoherent Scatter Observations, Grenoble, France, September 1982.

APPENDIX C

LIST OF RESEARCH PERSONNEL ACTIVE ON THE MITHRAS PROJECT

The following SRI International research personnel were active on the MITHRAS project:

M. Baron
O. de la Beaujardiere
J. Petriceks
C. Senior
C. Dawson
C. Leger

Through a subcontract to the MIT Haystack Observatory, the following personnel associated with the Millstone Hill radar were active on the MITHRAS project:

J. Evans
J. Holt
R. Wand
W. Oliver

In addition, P. Bauer from CNET, Paris, France spent two months at SRI International working on the MITHRAS data.

Other members of the scientific community have worked with the MITHRAS data, as mentioned in this report.


FIL